Fall 2014

Optimization in microgrid design and energy management

Tu Anh Nguyen

Department: Electrical and Computer Engineering

OPTIMIZATION IN MICROGRID DESIGN AND ENERGY MANAGEMENT

by

TU ANH NGUYEN

A DISSERTATION

Presented to the Faculty of the Graduate School of the

MISSOURI UNIVERSITY OF SCIENCE AND TECHNOLOGY

in Partial Fulfillment of the Requirements for the Degree

DOCTOR OF PHILOSOPHY

in

ELECTRICAL ENGINEERING

2014

Approved by

Dr. Mariesa L. Crow, Advisor
Dr. Jonathan Kimball
Dr. Mehdi Ferdowsi
Dr. Pourya Shamsi
Dr. Curt Elmore

PUBLICATION DISSERTATION OPTION

This dissertation has been prepared in publication format. Section 1.0, pages 1-3, has been added to supply background information for the remainder of the dissertation. Paper 1, pages 4-30, is entitled "Performance Characterization for Photovoltaic-Vanadium Redox Battery Microgrid Systems", and is prepared in the style used by the Institute of Electrical and Electronics Engineers (IEEE) Transactions on Sustainable Energy as published on March 21, 2014. Paper 2, pages 31-53, is entitled "Optimal Sizing of a Vanadium Redox Battery System for Microgrid Systems", and is prepared in the style used by the IEEE Transactions on Sustainable Energy as submitted on August 29, 2014. Paper 3, pages 54-77, is entitled "Stochastic Optimization of Renewable-based Microgrid Operation Incorporating Battery Operation Cost", and is prepared in the style used by IEEE Transactions on Sustainable Energy and will be submitted in December 2014.

ABSTRACT

The dissertation is composed of three papers, which cover microgrid systems performance characterization, optimal sizing for energy storage system and stochastic optimization of microgrid operation. In the first paper, a complete Photovoltaic-Vanadium Redox Battery (VRB) microgrid is characterized holistically. The analysis is based on a prototype system installation deployed at Fort Leonard Wood, Missouri, USA. In the second paper, the optimal sizing of power and energy ratings for a VRB system in isolated and grid-connected microgrids is proposed. An analytical method is developed to solve the problem based on a per-day cost model in which the operating cost is obtained from optimal scheduling. The charge, discharge efficiencies, and operating characteristics of the VRB are considered in the problem. In the third paper, a novel battery operation cost model is proposed accounting for charge/discharge efficiencies as well as life cycles of the batteries. A probabilistic constrained approach is proposed to incorporate the uncertainties of renewable sources and load demands in microgrids into the UC and ED problems.

ACKNOWLEDGMENT

I would like to express my deep gratitude to my advisor Dr. Mariesa L. Crow for her guidance, her caring and continuous support during my PhD program. I would like to sincerely thank Dr. Curt Elmore for his leadership and obtaining the grants to finance this research. I would also like to thank the other members of my committee, Dr. Jonathan Kimball, Dr. Mehdi Ferdowsi, and Dr. Pourya Shamsi for their guidance, time, and years of hard work at the Missouri University of Science and Technology.

Special thanks go out to my office mates .Maigha, Xin Qiu, Darshit Shah, Meng Fanjun and many others for their support and entertainment over my time at Missouri University of Science and Technology. I want to thank all members of my research group consisting of Jerry Tichenor, Joe Guggenberger, Thoshitha Gamage for their key support during the development of this project.

Finally, I would like to thank my Mom, Dad, family and friends for their constant support and encouragement during this process. Without them, none of this would be possible.

TABLE OF CONTENTS

LIST OF ILLUSTRATIONS

PAPER II

PAPER III

LIST OF TABLES

1. INTRODUCTION

During the past decades, the electric power industry has been reshaping in response to the rising concerns about global climate change and fast increasing fossil fuel prices. This trend has brought forth the concept of "Microgrid" which can be understood as a cluster of distributed energy resources, energy storage and local loads, managed by an intelligent energy management system (EMS). The microgrids exhibit many advantages over the traditional distribution systems such as energy losses reduction due to the proximity between DGs and loads, reliability improvement with the ability to work in islanded mode during system faults, transmission and distribution lines relief via efficient energy management to reduce energy import from the grid. For a more efficient, reliable and environmentally friendly energy production, it is critical to increase the integration of renewable energy resources (RE) in microgrids. Beside the advantages, the high integration of renewable energy also creates challenges to microgrids' design and operations.

Renewable power sources are typically highly variable depending on weather conditions, thereby necessitating the use of highly-efficient and rapid response energy storage systems (ESS) to store the surplus renewable energy and re-dispatch that energy when needed. Although many promising technologies are introduced to the consumer market, there's lack of information in the field to support them. Furthermore, most commercial chargers have been designed for lead acid batteries and when used with other energy storage technologies may adversely affect the round trip efficiency of the system. Therefore, there is still a gap that needs to be filled for characterizing the efficiencies and operating characteristics of new energy storage technologies.

Among the latest ESS technologies on the market, Vanadium Redox Battery (VRB) has shown lots of attractive features over the traditional battery storage: quick response, high efficiency, long life cycle, low self-discharge and easily estimated state of charge.

By proper control and scheduling of the VRB system, the microgrid operating costs can be significantly reduced. However, the initial capital and maintenance costs for the VRB are still relatively high in comparison to other energy storage systems (such as lead acid batteries). Therefore it is imperative to size and operate the VRB such that the reduction in operating costs can justify the increase in the capital investment.

As similar to the main grid operation, microgrid operation can be determined by unit commitment (UC) and economy dispatch (ED). The UC is performed from one day to one week ahead providing the start-up and shut-down schedule for each generation and storage unit which can minimize the operation cost of the microgrid. After UC is taken place, ED is performed from few minutes to one hour in advance to economically allocate the demand to the running units considering all unit and system constraints. Although the optimization of operation for the conventional power systems have been well studied in the literature, the proposed methods cannot be applied directly to microgrids with high integration of RE and ES devices. Specifically, due to the stochastic nature of the renewable resources such as solar and wind, the actual renewable power generation can be far different from the forecast values incurring extra operation cost for committing costly reserve units or penalty cost for curtailing the demands. In addition, to better utilize the renewable energy in the microgrid it is necessary to charge/discharge and coordinate the energy storage units in an efficient and economical way.

To address the above problems, three journal papers have been proposed in this dissertation:

In the first paper, a complete Photovoltaic-Vanadium Redox Battery (VRB) microgrid is characterized holistically. The analysis is based on a prototype system installation deployed at Fort Leonard Wood, Missouri, USA. Specifically, the characterization of the PV-VRB microgrid performance under different loading and weather conditions; the development of a two-stage charging strategy for the VRB, and a quantification of the component efficiencies and their relationships.

In the second paper, the optimal sizing of power and energy ratings for a VRB system in isolated and grid-connected microgrids is proposed. An analytical method is developed to solve the problem based on a per-day cost model in which the operating cost is obtained from optimal scheduling. The charge, discharge efficiencies, and operating characteristics of the VRB are considered in the problem. Case studies are performed under different conditions of load and solar insolation.

In the third paper, a novel battery operation cost model is proposed accounting for charge/discharge efficiencies as well as life cycles of the batteries. The model allows to treat a battery as an equivalent fossil fuel generator in the Unit Commitment (UC) and Economy Dispatch (ED). A probabilistic constrained approach is proposed to incorporate the uncertainties of renewable sources and load demands in microgrids into the UC and ED problems. The UC is solved using stochastic dynamic programming.

I. PERFORMANCE CHARACTERIZATION FOR PHOTOVOLTATIC-VANADIUM REDOX BATTERY MICROGRID

Tu A. Nguyen, Xin Qiu, Joe D. Guggenberger*, M. L. Crow, *IEEE Fellow*, and A. C. Elmore*

Department of Electrical and Computer Engineering

*Department of Geological Engineering

Missouri University of Science and Technology, Rolla, MO 65401

Abstract

The integration of photovoltatics (PV) and vanadium redox batteries (VRB) in microgrid systems has proven to be a valuable, environmentally-friendly solution for reducing the dependency on conventional fossil fuel and decreasing emissions. The integrated microgrid system must be characterized to develop appropriate charging strategies specifically for VRBs, sizing microgrid systems to meet a given load, or comparing the VRB to other energy storage technologies in different applications. This paper provides a performance characterization analysis in a PV-VRB microgrid system for military installations under different conditions of load and weather. This microgrid system is currently deployed at the Fort Leonard Wood army base in Missouri, USA.

Index Terms

Microgrid, renewable energy, energy storage, vanadium redox battery, efficiency characterization

I. INTRODUCTION

Microgrids with integrated renewable resources are emerging as a solution for reducing the dependency on conventional fossil fuel and reducing emissions in distribution systems. The variability of renewable power sources requires quick response and highly

efficient storage devices with larger power and energy density, which creates a challenge in developing renewable energy-based microgrids in large scale. To obtain the optimal performance from an integrated renewable energy, the round trip efficiency of the entire system must be characterized. Although many new energy storage technologies are reaching the consumer market, there is little field experience to support their adoption. Furthermore, most commercially available charging systems have been designed for lead acid batteries and when used with other energy storage technologies may adversely affect the round trip efficiency of the system. Thus the energy storage system may not reflect the manufacturer's predicted performance. Therefore in this paper, we fully characterize the round trip efficiency of a photovoltaic (PV) system that uses a vanadium redox battery to provide increased confidence in their deployment.

The Vanadium Redox Battery (VRB) is a relatively new commercially available energy storage system. The vanadium redox battery energy storage system is an electrical energy storage system based on the vanadium-based redox regenerative fuel cell that converts chemical energy into electrical energy. The VRB differs from traditional battery storage in that the amount of energy it can store is independent of its power rating. The size of the stack determines the power rating whereas the amount of electrolyte determines the energy capacity. Thus the energy rating of the VRB can be changed "on the fly" by increasing or decreasing the amount of electrolyte in the storage tanks. Furthermore, the VRB can be stored for long periods of time without charge degradation.

Due to its recent commercialization, the information available in the literature on VRB-based microgrids is limited. Most work has focused on electrochemical and electrical modeling of the VRB, [1–4], on electrode, electrolyte, and membrane materials characterization [5, 6], or on optimal VRB pump operation [7]. Only recently has the VRB been considered for microgrid applications. In [8], the VRB-based microgrid performance was predicted based on geographic location, weather data and loading conditions; however, the effect of the charging/discharging voltage levels and VRB internal losses on system efficiency were neglected.

In this paper, a complete PV-VRB microgrid is characterized holistically. The analysis is based on a prototype system installation deployed at Fort Leonard Wood, Missouri, USA. Specifically, the following contributions are made in this paper:

- the characterization of the PV-VRB microgrid performance under different loading and weather conditions,
- the development of a two-stage charging strategy for the VRB, and
- a quantification of the component efficiencies and their relationships.

II. MICROGRID SYSTEM DESCRIPTION

The microgrid system had been constructed to serve a standalone 5 kW (maximum) AC load in a single building. As shown in Fig. 1, the electrical system is designed with a 48 VDC bus and a 120 VAC split-phase bus. The PV arrays and VRB are connected to the DC bus whereas the utility grid and load circuits are connected to the AC bus through a transfer switch. The inverter links the two buses to power the load on the AC side by using renewable energy from the DC side. A PLC-controlled transfer switch is used to connect the load to the grid when the renewable energy is not available and the energy storage is depleted.

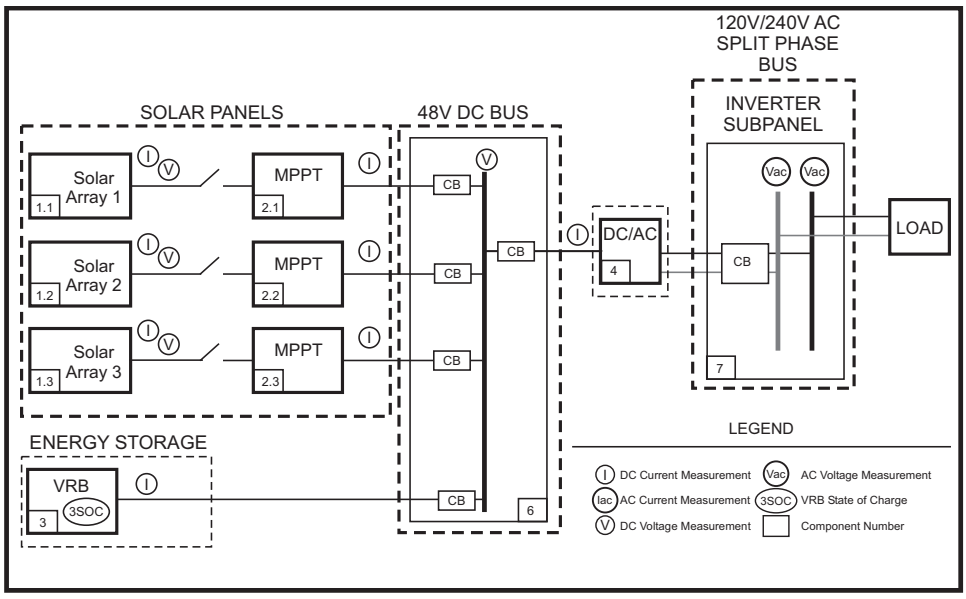

Fig. 1: One-line diagram of the microgrid system

The PV array is constructed from 54 280 W solar panels (model Suntech STP280-24/Vd) for a composite rating of 15 kW. The system is electrically divided into three 5 kW PV arrays which are south facing and tilted at a fixed angle of 38° to match the latitude of Fort Leonard Wood. Each of the arrays is connected to the DC bus through an Outback FlexMax 80 MPPT/charge controller to track the PV maximum power point.

A 38-cell Prudent Energy VRB rated 5 kW/20 kWh is used for energy storage. The capacity range of the VRB is specified as 20kWh at a SOC of 73% and 0kWh at a SOC of 20%. It can be charged to a maximum voltage of 56.5 V and discharged to a minimum voltage of 42 V. The VRB energy storage system is self-contained in an enclosure and includes the electrolyte tanks, cell stacks, pumps, and controllers. The enclosure temperature is regulated between 10° C and 30° C via an external heating, ventilation, and air conditioning (HVAC) system.

The system is instrumented to measure environmental data including solar insolation and temperature as well as the voltage and current parameters necessary for monitoring, controlling its operation and characterizing its performance. Operational data was are recorded using Campbell Scientific Model CR3000 and CR1000 dataloggers which sample every $5s$ and average the values every $1min$.

III. VANADIUM REDOX BATTERIES PERFORMANCE CHARACTERIZATION

A vanadium redox battery (shown in Fig. 2) is a flow-type battery that stores chemical energy and generates electricity by reduction-oxidation (redox) reactions between different ionic forms of vanadium in the electrolytes [4]. The batteries are comprised of two closed electrolyte circuits. In each circuit, the electrolyte is stored in a separate tank and circulated via pumps through the cell stacks where the electrochemical reactions (1)-(2) occur [9]. Table I contains a list of all nomenclature used in this section.

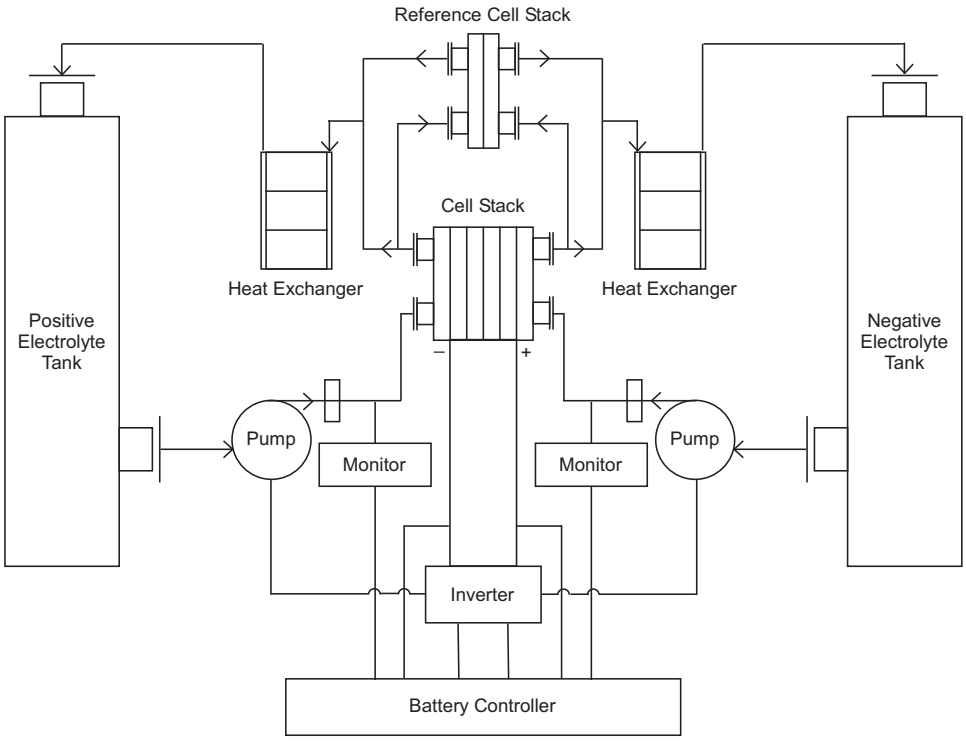

Fig. 2: VRB schematic diagram

$$VO_2^+ + 2H^+ + e^- \underset{c}{\overset{d}{\rightleftharpoons}} VO^{2+} + H_2O \tag{1}$$

$$V^{2+} \underset{c}{\overset{d}{\rightleftharpoons}} V^{3+} + e^- \tag{2}$$

The catholyte contains VO^{2+} and VO_2^+ ions and the anolyte contains V^{3+} and V^{2+} ions suffused in a H_2SO_4 solution. During discharge, V^{2+} is oxidized to V^{3+} in the negative half-cell producing electrons and protons. Protons diffuse through the membrane while the electrons transfer through the electrical external circuit to the positive half-cell where VO_2^+ is reduced to VO^{2+}. The redox process occurs in reverse during the charge cycle.

TABLE I: Nomenclature

N_c	Number of cells in VRB stack
C_x	Concentration of the species x in the electrolyte (mol/l)
V_{stack}	VRB stack voltage at terminals (V)
V_{oc}	VRB open-circuit voltage (V)
E_o	VRB standard potential (V)
V_{loss}	VRB internal voltage loss
ΔG_o	Gibbs free enthalpy at standard condition (kJ/mol)
ΔH_o^r	Reaction enthalpy at standard condition (-155.6 kJ/mol)
ΔS_o^r	Reaction entropy at standard condition (-121.7 J/mol K)
F	Faraday constant (96485.3365 s A/mol)
R	Universal gas constant (8.3144621 J/mol K)
T	Electrolyte temperature ($^\circ K$)
T_{en}	VRB enclossure temperature ($^\circ C$)
T_{amb}	Ambient temperature ($^\circ C$)
I_{stack}	VRB stack acurrent (A)
P_{load}	VRB load power (kW)
P_{charge}	VRB charge power (kW)
P_{stack}	VRB load power at terminal (kW)
P_{pump}	VRB pump power (kW)
P_{AC}	Air conditioner power (kW)
η_v	VRB efficiency with internal voltage loss
η_p	VRB efficiency with parasitic loss
η_d^{VRB}	VRB total discharge efficiency
η_c^{VRB}	VRB total charge efficiency

A. VRB State of Charge and Open-Circuit Voltage

The VRB charge and discharge operations depend on the state of charge, the load, and the power produced by the PV array. The VRB's state of charge is defined by the ratio of the concentration of unoxidized vanadium (V^{2+}) to the total concentration of vanadium (C_V). This is also the same as the ratio of vanadium oxide ($C_{VO_2^+}$) to the total concentration (3):

$$SOC = \frac{C_{V^{2+}}}{C_V} = \frac{C_{VO_2^+}}{C_V} \tag{3}$$

The total concentration of vanadium is the sum of the vanadium ions which is the

same as the sum of the vanadium oxide ions (4):

$$C_V = C_{V^{2+}} + C_{V^{3+}} = C_{VO_2^+} + C_{VO^{2+}} \tag{4}$$

The SOC can be calculated from the VRB open-circuit voltage (V_{oc}) of a reference cell stack which uses the same electrolyte as the main stack. The open-circuit voltage (or the equilibrium potential) is the highest potential that the VRB can provide without any losses. It can be determined by the complete form of Nernst's equation [10]:

$$\begin{aligned} V_{oc} = E_o + \frac{RT}{F} \ln \left\{ \left(\frac{C_{VO_2^+} (C_{H^+})^3}{C_{VO^{2+}}} \right)_{\text{catholyte}} \right\} \\ + \frac{RT}{F} \ln \left\{ \left(\frac{C_{V^{2+}}}{C_{V^{3+}} C_{H^+}} \right)_{\text{anolyte}} \right\} \end{aligned} \tag{5}$$

where

- E_o is free Gibbs potential where:

$$\begin{aligned} E_o(T) = -\frac{\Delta G_o}{nF} = -\frac{\Delta H_o^r - T\Delta S_o^r}{F} \\ = 1.61268 - 0.00126T, \end{aligned} \tag{6}$$

- T is the electrolyte temperature,
- R is the universal gas constant,
- F is the Faraday constant,
- $H_\circ^T$ ($S_\circ^T$) is the reaction enthalpy (entropy), and
- the concentrations of vanadium ions can be found from (3) and (4):

$$C_{V^{2+}} = C_{VO_2^+} = C_V SOC \tag{7}$$

$$C_{V^{3+}} = C_{VO^{2+}} = C_V(1 - SOC) \tag{8}$$

Combining (5), (6), (7), and (8), the open-circuit voltage of a single cell can be

expressed as a function of SOC and temperature:

$$V_{oc} = 1.61268 - 0.00126T + 1.72 \times 10^{-4} T \ln\left(\frac{SOC}{1 - SOC}\right) + 1.72 \times 10^{-4} T \ln\left(f(SOC)\right) \quad (9)$$

where $f(SOC)$ is an emperically determined function of state of charge. The manufacturer data sheet provides a SOC versus V_{oc} at $25°C$. By fitting a curve through the manufacturer's data, $f(SOC)$ can be found with a fitness (R^2) of 0.999:

$$f(SOC) = -154.2SOC^3 + 264.7SOC^2 - 95.4SOC + 30.7 \quad (10)$$

Fig. 3 shows a series of traces calculated at different temperatures of the single-cell open-circuit voltage as a function of SOC using the function in (10). The upper curve is measured at temperature of $5°C$ and each lower trace is for an increase of $5°C$ to the bottom trace which is for $T = 35°C$. In the area between $SOC = 0.1$ and $SOC = 0.83$, V_{oc} and SOC can be linearly correlated, therefore the single-cell $V_{oc}(T, SOC)$ in linear region can be characterized as:

$$V_{oc}(T, SOC) = \frac{T}{1000}(SOC - 1.1755) + 1.6123 \quad (11)$$

Since the working region of the VRB lies within the linear region (as a function of temperature), this relationship will be used when calculating the system efficiency.

B. VRB Discharge Performance

During discharge, the VRB supplies power to the load and to its own pumps as shown in Fig. 4. To characterize the discharge performance of the VRB, the stack voltage, the internal voltage losses and the parasitic losses are correlated to the stack current, the load power, and the SOC and temperature.

1) VRB stack voltage and internal voltage loss: The VRB cell stack is composed of 38 cells in series. Due to the internal voltage losses, the VRB stack voltage is lower at higher discharge current. The stack voltage is approximately proportional to the stack current at

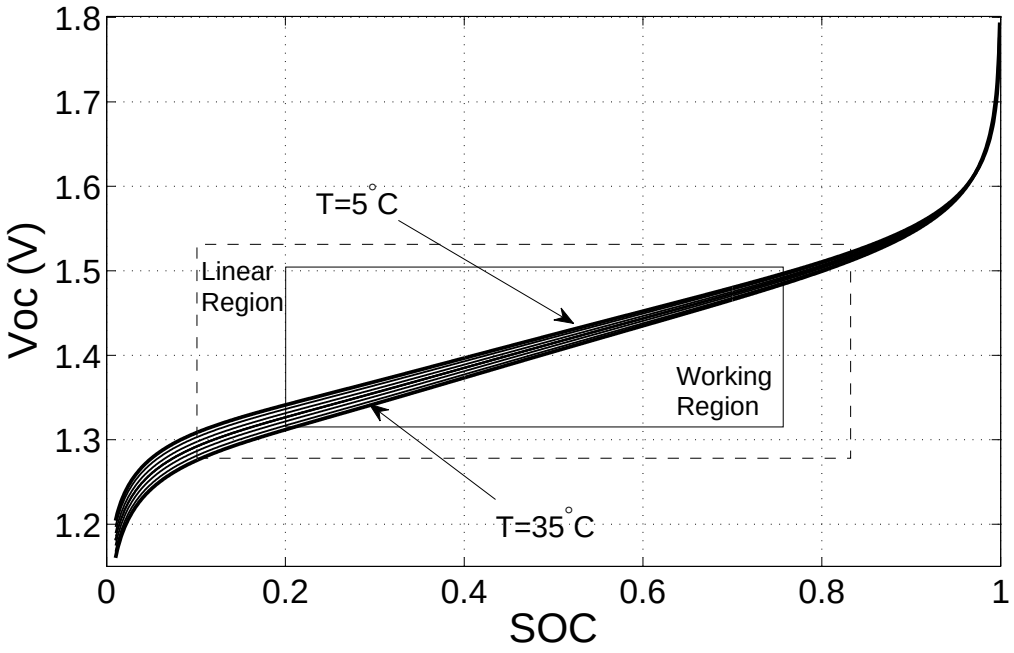

Fig. 3: VRB open-circuit voltage as a function of SOC and temperature

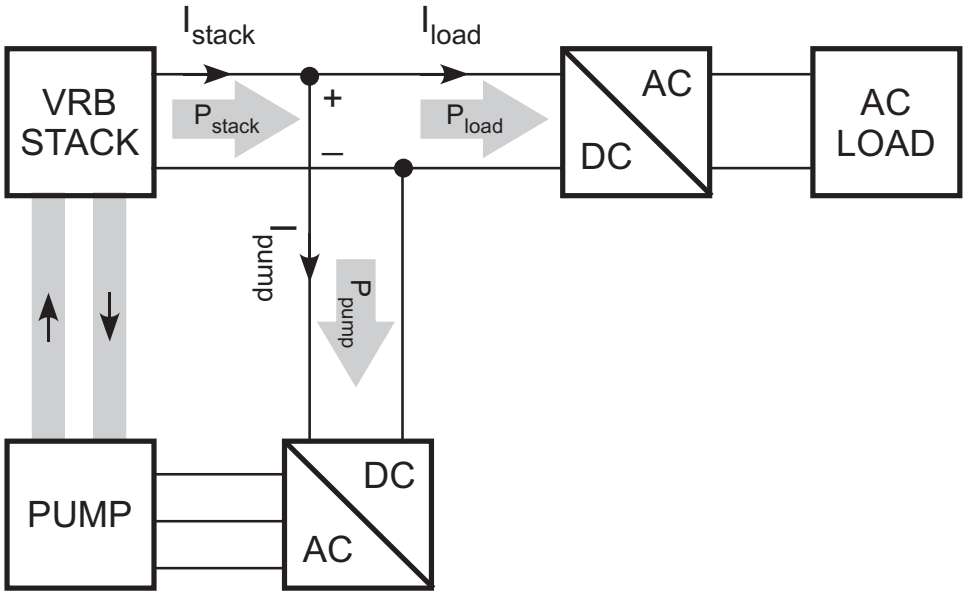

Fig. 4: Power flow in VRB storage system during discharge

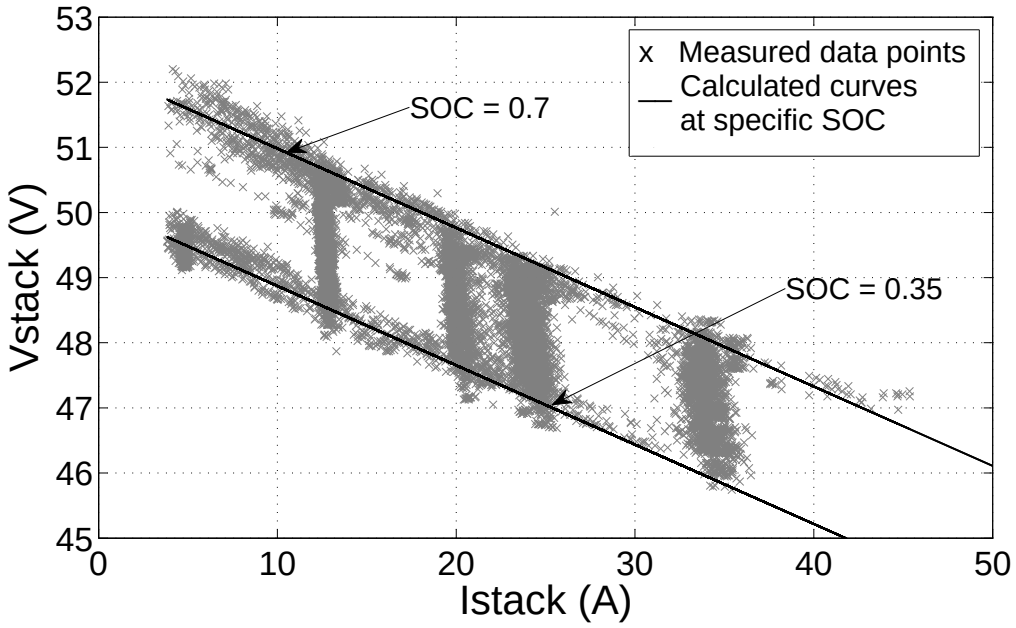

Fig. 5: Discharge voltage at different SOC

different values SOC. Fig. 5 shows the relationship between stack voltage and current at different SOCs. The clustering of measured data points at certain current levels is due to the system load; several of the load components are discontinuous "on/off" (compressor) loads, therefore a large portion of the load current jumps between set points thereby causing the data points to cluster. Note that the data falls within a linear envelope that is defined by the upper and lower SOC boundaries. For a given SOC, a linear fit can be found between the stack voltage and current (12). The solid lines in Fig. 5 show the calculated relationship at the upper and lower SOC range.

$$V_{stack} = -0.1218 I_{stack} + 6.5926 SOC + 47.601 \tag{12}$$

Similarly, the stack voltage can be related to the load:

$$V_{stack} = -2.72 P_{load} + 6.3606 SOC + 47.335 \tag{13}$$

By combining (11) and (12), the total voltage drop due to the VRB internal losses

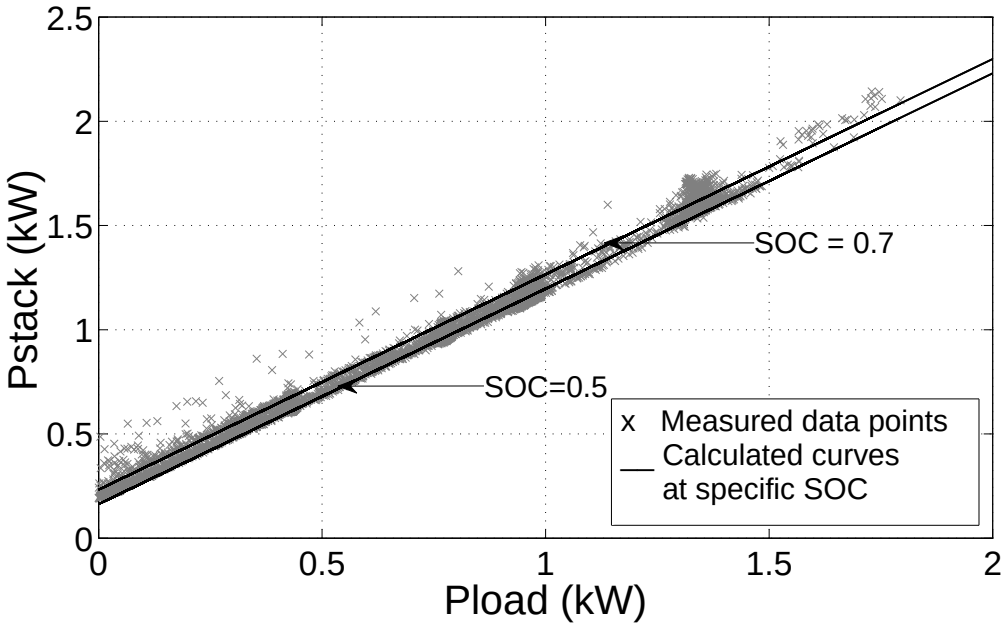

Fig. 6: Discharge stack power at different SOC

can be expressed as:

$$\begin{aligned} V_{loss} &= V_{oc} - V_{stack} = V_{ohm} + V_{act,conc} \\ &= 0.1218 I_{stack} + 0.038T(SOC - 1.1755) \\ &\quad - 6.5926SOC + 13.6664 \end{aligned} \tag{14}$$

where

- $V_{ohm} = 0.1218 I_{stack}$ represents the ohmic losses due to the internal resistance of the VRB, and
- $V_{act,conc} = 0.038T(SOC - 1.1755) - 6.5926SOC + 13.6664$ represents the activation and concentration losses caused by charge transfer initiation and concentration difference between the bulk electrolyte and the electrode surface [4].

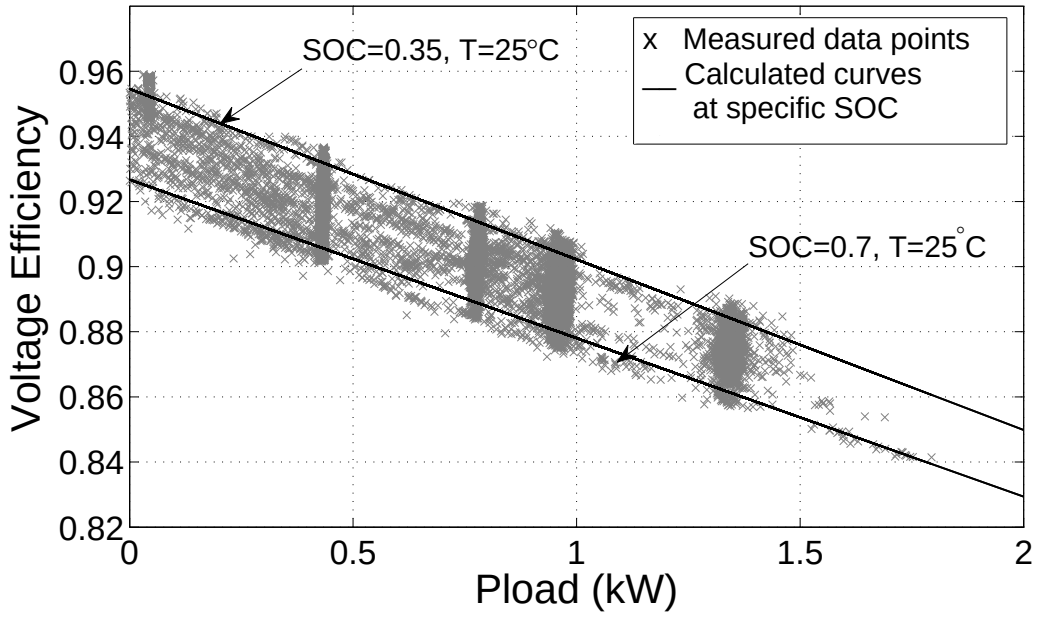

Fig. 7: Discharge voltage efficiency at different SOC

2) VRB parasitic losses: As shown in Fig. 6, the stack power is approximately linear to the load power at a given SOC:

$$P_{stack} = 1.0334P_{load} + 1.727SOC^2 - 1.737SOC + 0.596 \tag{15}$$

The parasitic loss is the power required to run the pumps and the controller of the VRB. It is calculated as the difference between the stack power and the load power:

$$\begin{aligned} P_{pump} &= P_{stack} - P_{load} \\ &\approx 0.0334P_{load} + 1.727SOC(SOC-1) + 0.596 \end{aligned} \tag{16}$$

Note that at a specific load, the parasitic power is a quadratic function of SOC and its minimum occurs when the SOC is approximately 0.5.

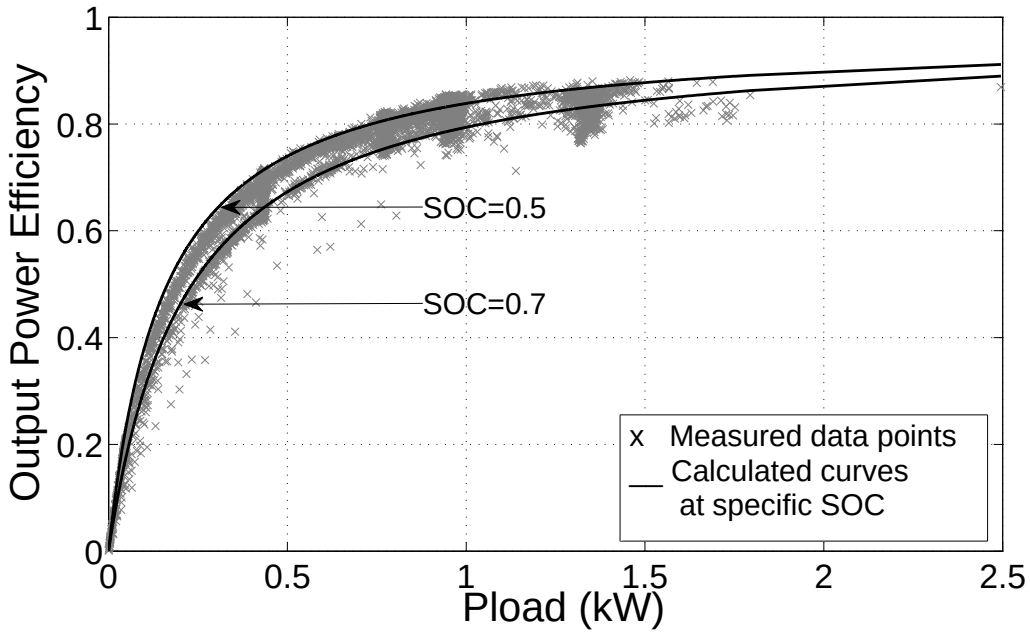

Fig. 8: Discharge power efficiency at different SOC and temperature

3) VRB discharge efficiency: The efficiency of the VRB storage system during discharge is

$$\eta_d^{\boldsymbol{VRB}} = \frac{P_{load}}{P_{VRB}} \tag{17}$$

$$= \frac{P_{load}}{P_{stack}} \frac{P_{stack}}{P_{VRB}} \tag{18}$$

However, since P_{stack} and P_{VRB} have the same current, this is the same ratio as the voltages. Therefore

$$\eta_d^{\boldsymbol{VRB}} = \frac{P_{load}}{P_{stack}} \frac{V_{stack}}{V_{oc}} \tag{19}$$

$$= \eta_d^p \eta_d^v \tag{20}$$

where

- η_d^v is the "voltage efficiency" which accounts for the internal ohmic losses. From (11) and (12), it is a function of load power, SOC and temperature (Fig. 7):

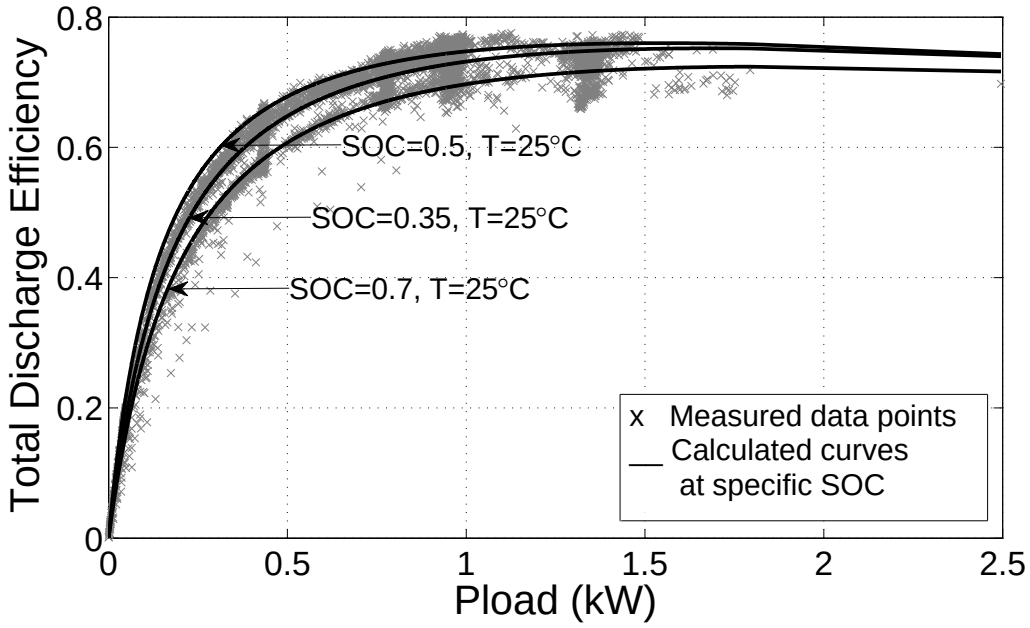

Fig. 9: VRB total discharge efficiency at different SOC and temperature

$$\eta_d^v = \frac{V_{stack}}{V_{oc}} = \frac{-2.72P_{load} + 6.3606SOC + 47.335}{0.038T(SOC - 1.1755) + 61.2674} \tag{21}$$

- η_d^p is the output power efficiency which accounts for the parasitic losses. From (15), it is characterized as a function of load power and SOC (Fig. 8):

$$\begin{aligned} \eta_d^p &= \frac{P_{load}}{P_{stack}} \\ &= \frac{P_{load}}{1.0334P_{load} + 1.727SOC(SOC - 1) + 0.596} \end{aligned} \tag{22}$$

The combined efficiencies are shown in Fig. 9. Note that the total discharge efficiency is maximum when the SOC is 0.5 with a maximum discharge efficiency of 78%. The VRB is most efficient under heavy load and is dominated by the parasitic losses as opposed to the ohmic losses. This is due to the pumps having to circulate the electrolyte even during low discharge currents.

4) Inverter efficiency: During discharge, the VRB supplies power to the AC load through an inverter. From measured operation, the linear correlation between the input and the output power of the inverter was fit resulting in (23) with $R^2 = 0.988$.

$$P_{load}^{ac} = 0.991 P_{load}^{dc} - 0.0574 \tag{23}$$

The inverter efficency is therefore characterized:

$$\eta_{INV} = 0.991 - \frac{0.0574}{P_{load}^{dc}} = 0.991 - \frac{0.0574}{1.0091 P_{load}^{ac} + 0.0579} \tag{24}$$

C. VRB Charge Performance

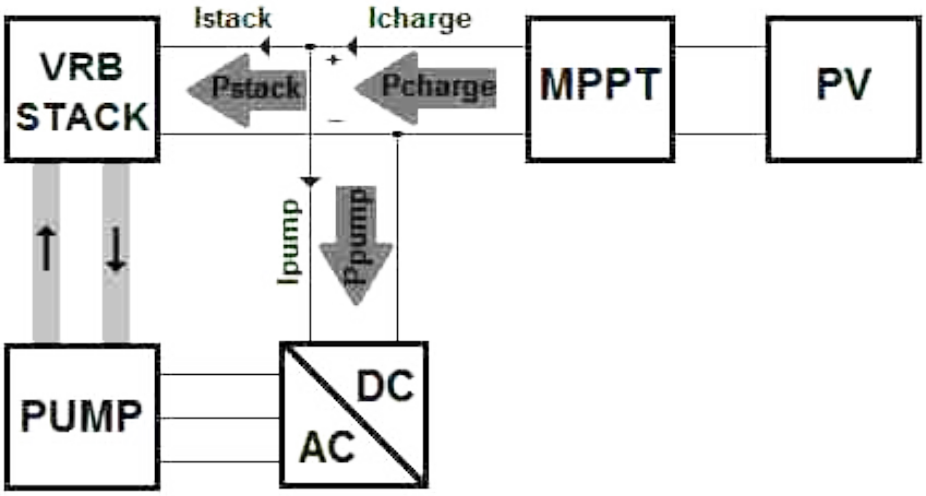

Fig. 10: Power flow in VRB storage system during charge

In the microgrid system, the power from the PV arrays is used to charge the VRB storage system. When PV power is available, but not high enough to run the VRB pumps, the VRB cannot start to charge, therefore the charging current is zero. The parasitic power is around $500W$ to maintain the minimum flow rate of the electrolyte. When the available PV power is higher than the parasitic power, the VRB will start to charge. Commercially available battery chargers operate by charging in one of several modes to avoid overcharging the battery. Furthermore, many charge controllers for PV-battery systems also include a

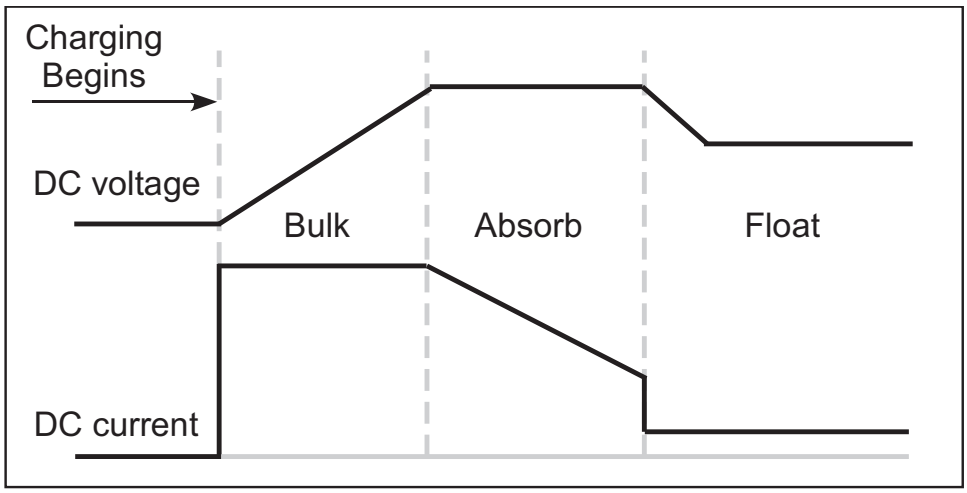

Fig. 11: Typical battery charge regions

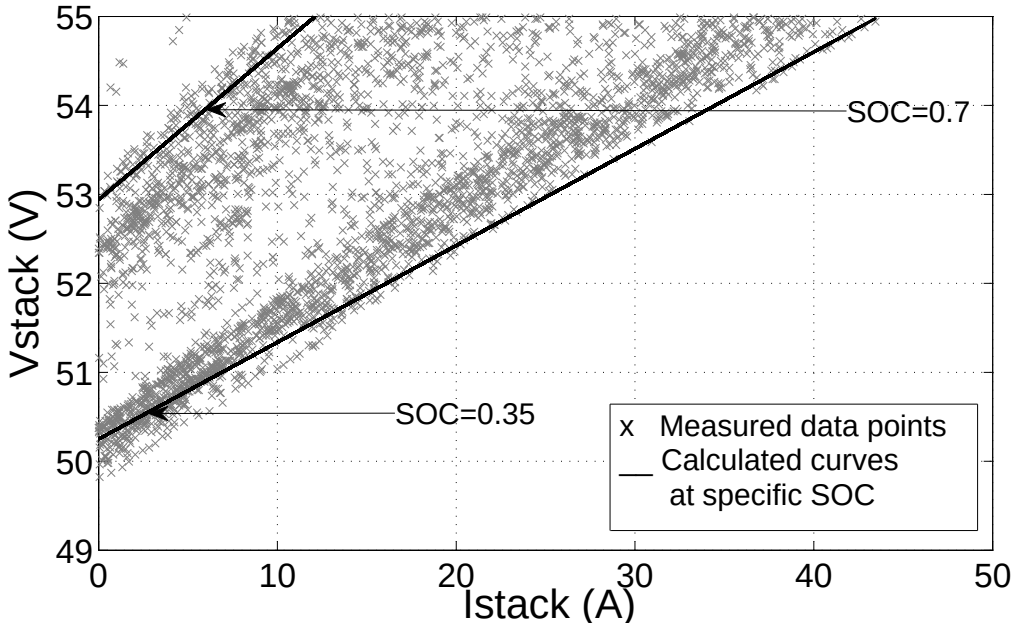

Fig. 12: Charge voltage at different SOC

maximum power point tracker (MPPT) to extract the maximum power from the PV panels. These regions are shown in Fig. 11 and summarized:

- Bulk: when the VRB stack voltage is lower than the *absorb* voltage, the MPPT/charge controller tracks the maximum PV power and charges the VRB with the maximum

current. The *absorb* voltage level can be set by the user at different levels from $55V$ to $56.5V$.

- Absorb: when the VRB stack voltage reaches the *absorb* voltage set point, the MPPT/charge controller regulates the stack voltage and charges the VRB at a constant voltage.

1) VRB bulk stage: During the *bulk* stage, the larger current the current produced by the PV, the faster the VRB is charged. Fig. 12 shows that the stack voltage in *bulk* stage is approximately linear to the stack current. The (V_{stack}, I_{stack}) and (V_{stack}, P_{charge}) correlations are given by:

$$V_{stack} = (0.166SOC + 0.054)I_{stack} + 7.27SOC + 47.85 \tag{25}$$

$$V_{stack} = (1.895SOC + 1.552)P_{charge} + 6.82SOC + 46.79 \tag{26}$$

Combining (11) and (25), the internal voltage loss is characterized as a function of the stack current and SOC in (27). In this case, the internal resistance is linear to the SOC due to the ionic effect which opposes the flow of charges in the electrolyte and the membrane [4].

$$\begin{aligned} V_{loss} &= V_{stack} - V_{oc} \\ V_{loss} &= (0.166SOC + 0.054)I_{stack} + 7.27SOC \\ &\quad - 0.038T(SOC - 1.1755) - 13.42 \end{aligned} \tag{27}$$

2) VRB absorb stage: In the *absorb* stage, the stack voltage is regulated to be constant at the *absorb* setpoint voltage to avoid damaging the VRB. The stack current is limited by the potential difference between the equilibrium potential (open-circuit voltage) and the stack voltage. Fig. 13 shows the dependence of the *absorb* power on the SOC and *absorb* voltage. Note that in the *bulk* region, the charge power varies considerably as a function of the PV panel output.

The (I_{stack}, SOC) and (P_{charge}, SOC) linear correlations at different settings of *absorb* voltage. The stack current and the absorb power are specified as functions of SOC

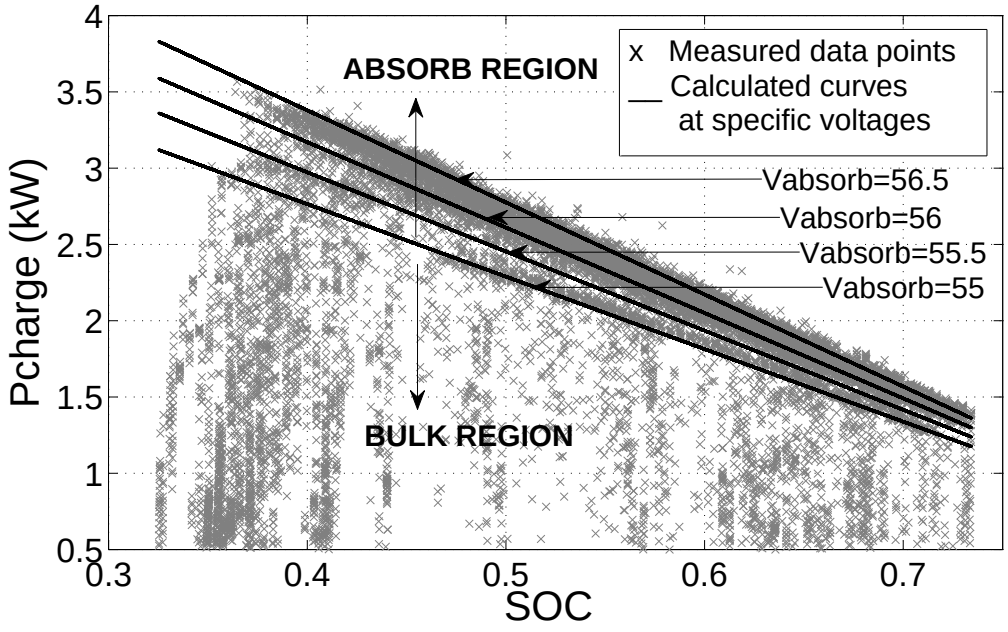

Fig. 13: Maximum power at different absorb voltage

and *absorb* voltage as below:

$$\begin{aligned} P_{stack} =&(-0.874V_{stack}^{ab} + 43.317)SOC \\ &+ 0.767V_{stack}^{ab} - 37.52 \end{aligned} \tag{28}$$

$$\begin{aligned} I_{stack} =&(-14.543V_{stack}^{ab} + 714.47)SOC \\ &+ 12.616V_{stack}^{ab} - 619.38 \end{aligned} \tag{29}$$

The lower the SOC and the higher the *absorb* voltage setpoint are, the higher the charge current and power that the VRB can absorb. This VRB charging behavior is similar to that of lead-acid batteries. Therefore, the *absorb* voltage should be set at the maximum of $56.5V$.

3) VRB parasitic loss: When the VRB is charged, the pumps are controlled to produce the maximum electrolyte flow rate. The parasitic losses in this case can be calculated as the difference between the charge power and the stack power. The linear correlations

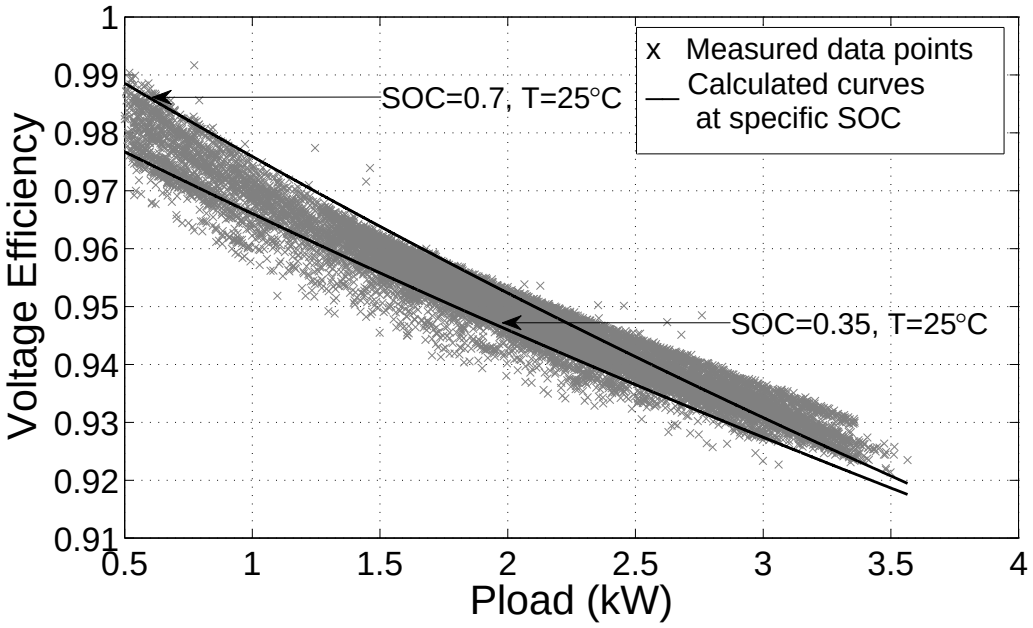

Fig. 14: Charge voltage efficiency at different SOC and temperature

between P_{stack} and P_{charge} at different SOC are characterized as:

$$P_{stack} = (-0.128SOC + 1.05)P_{charge} + 0.19SOC - 0.59 \tag{30}$$

$$\begin{aligned} P_{pump} &= P_{charge} - P_{stack} \\ &\approx (0.128SOC - 0.05)P_{charge} - 0.19SOC + 0.59 \end{aligned} \tag{31}$$

4) VRB charge efficiency: Similar to the discharge efficiency, the charge efficiency of the VRB storage system is calculated based on the voltage efficiency and the input power efficiency:

$$\eta_c^{VRB} = \eta_c^v \eta_c^p \tag{32}$$

in which

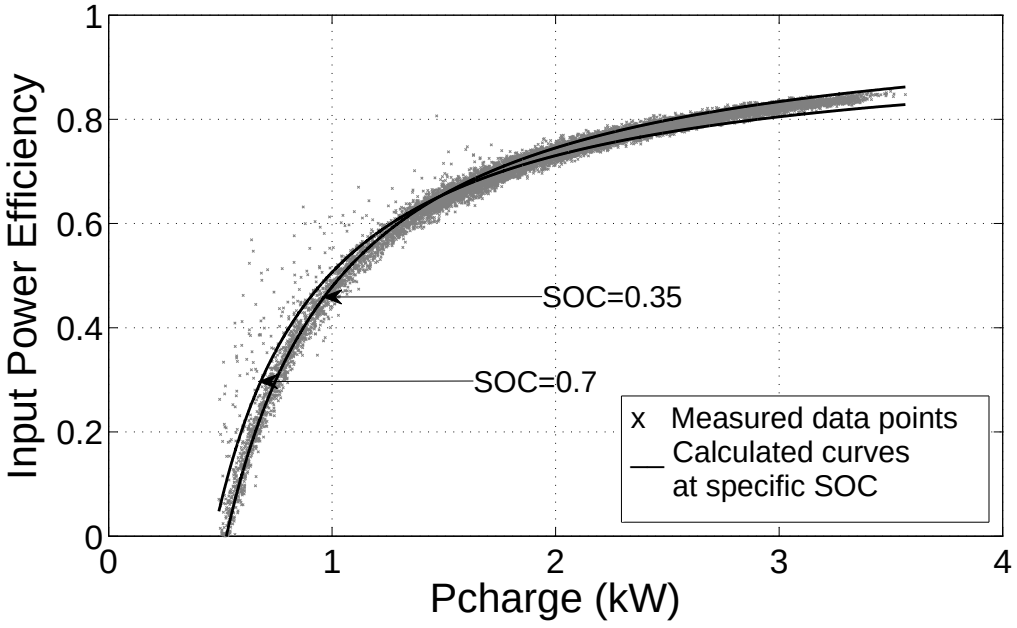

Fig. 15: Charge power efficiency at different SOC

- the voltage efficiency η_c^v can be found based on (11) and (26)

$$\begin{aligned}\eta_c^v &= \frac{V_{oc}}{V_{stack}} \\ &= \frac{0.038T(SOC - 1.1755) + 61.2674}{(1.895SOC + 1.552)P_{charge} + 6.82SOC + 46.79}\end{aligned} \tag{33}$$

- the input power efficiency η_c^p can be specified from (30)

$$\begin{aligned}\eta_c^p &= \frac{P_{stack}}{P_{charge}} \\ &= \frac{(-0.128SOC + 1.05)P_{charge} + 0.19SOC - 0.59}{P_{charge}}\end{aligned} \tag{34}$$

As shown in Fig. 16, the maximum charge efficiency is around 80%. When the available PV power is less than 500W, the charge efficiency is zero due to the VRB parasitic loss.

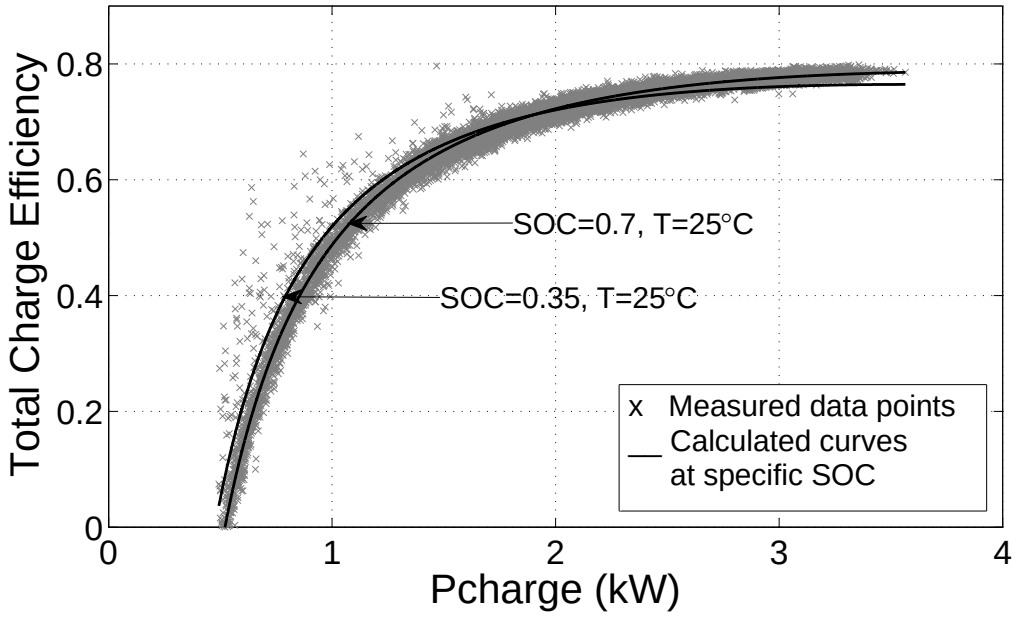

Fig. 16: VRB total charge efficiency at different SOC and temperature

5) MPPT charger efficiency: The MPPT chargers are used to track the maximum PV power and charge the VRB. The MPPT input and output power are correlated in (35):

$$P_{MPPT}^{out} = 0.989 P_{MPPT}^{in} - 0.124 \tag{35}$$

The MPPT efficiency is specified as:

$$\eta_{MPPT} = \frac{P_{MPPT}^{out}}{P_{MPPT}^{in}} = 0.989 - \frac{0.124}{1.0111 P_{MPPT}^{out} + 0.1253} \tag{36}$$

D. VRB Heating Ventilation and Air Conditioning (HVAC)

Enviromental controls are required for the VRB storage system to operate properly. Freezing temperatures can hinder electrolyte flow, whereas high temperatures can damage the VRB membrane and cause overheating of the electrical equipment. In this system, VRB enclosure temperature is regulated between $10°C$ and $30°C$ by a built-in HVAC system that includes a cooling-heating air conditioner and ventilation fans. The temperature control scheme is:

- Heating is ON when the enclosure temperature is lower than $10°C$.
- Fans are ON when the enclosure temperature is between $25°C$ and $30°C$.
- Cooling is ON when the enclosure temperature is greater than $30°C$.

The fans' load is a constant $300W$. The air conditioner load had been characterized in [8] as:

$$P_{AC} = (0.00313)|T_{en}(T_{amb} - T_{en})| + 0.4125 \tag{37}$$

where T_{en} is the VRB enclosure temperature and T_{amb} is the external ambient temperature.

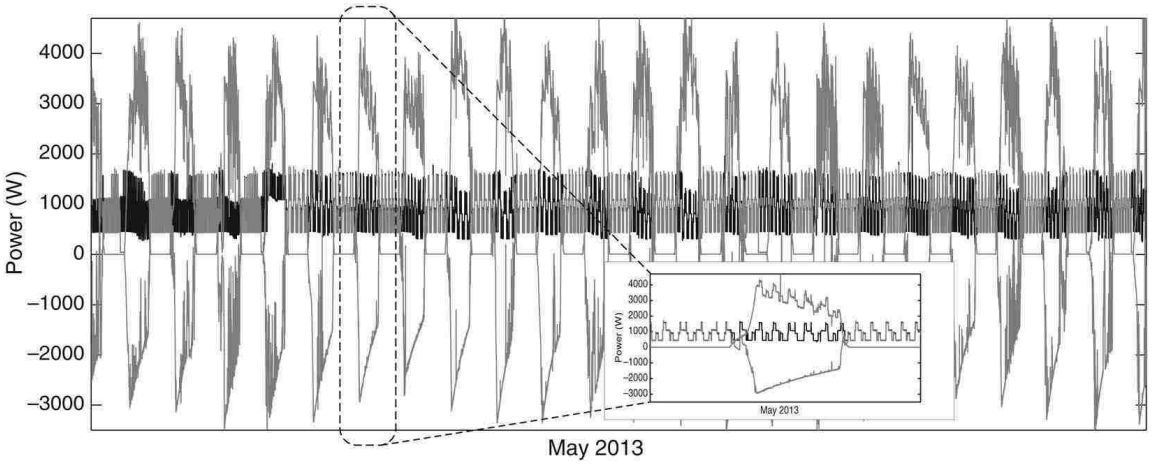

Fig. 17: Microgrid system performance in May 2013

IV. MICROGRID SYSTEM PERFORMANCE

The microgrid system is designed to operate in either a *grid* or *renewable* mode.

- Renewable mode: the load is powered by the VRB and by available PV power. This mode occurs when VRB is serving the load and the $SOC > 0.35$, or when there is sufficient PV power and the VRB is charging and $SOC > 0.55$. The system switches from this mode to *grid* mode when the VRB is discharging and the SOC falls below 0.35.
- Grid mode: the load is powered by the utility grid and the VRB is charged by available PV power. The system remains operating in this mode until the VRB SOC reaches 0.65.

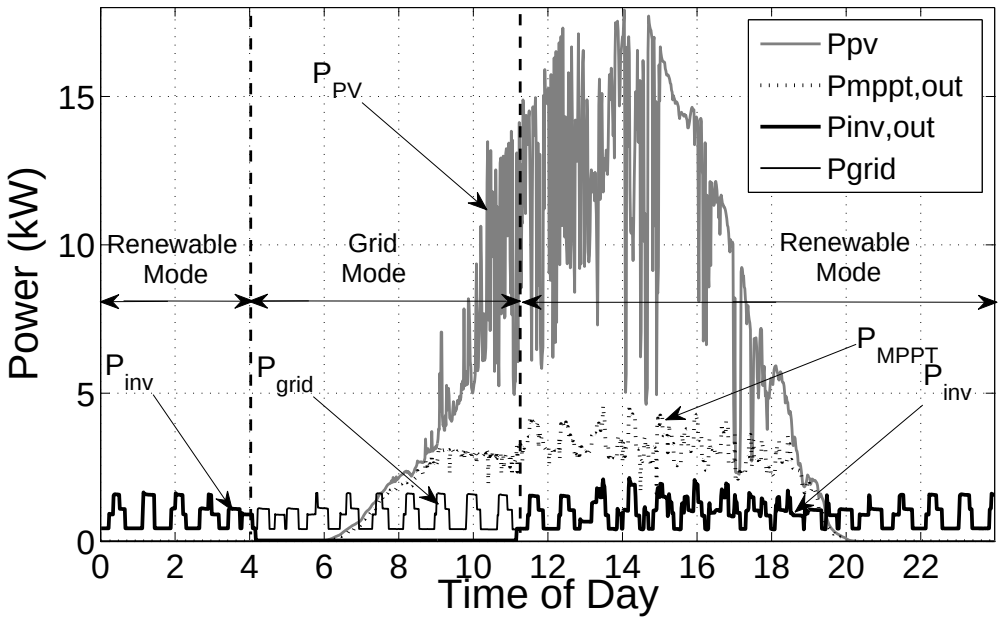

Fig. 18: PV and load power profile on 7 May 2013

The system operating characteristics and efficiencies can be predicted based on SOC, charge power and load power as presented in Section III. A case study has been performed based on field data taken in May 2013. During this period, the system is serving a 2 kW (peak) load. The inputs of the prediction model are daily load power profile, available PV power profile and the initial SOC. At each time step (1 min), the system operating characteristics, the losses in the system, transfer switch status, and SOC are updated. The measured performance for the month of May 2013 is shown in Fig. 17. The upper trace is the power from the charge controller, the lower trace is the power from the VRB (negative indicates charging), and the middle black trace is the load power. A typical day is shown in the inset to provide greater detail.

The actual cumulative data and predicted data of a typical day in May (7 May) have been plotted in Figs. 18-21. Note that this was a sunny day with intermittent cloud cover. The effect of the compressor load can be clearly seen in the various powers. From the results, whole-day period can be analyzed in three main periods as indicated in Fig. 18:

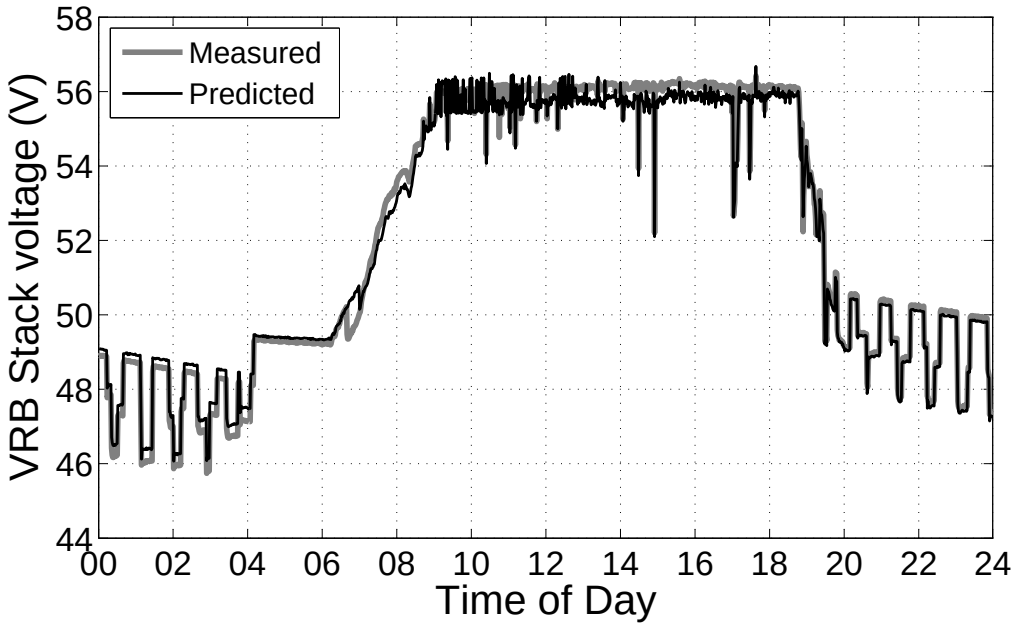

Fig. 19: VRB stack voltage on 7 May 2013

- *Period 1* is from midnight to 04:00 during which time there is no PV power and the VRB is discharging to power the load (as indicated by the P_{inv} trace which denotes the power from the inverter). The VRB output voltage (in Fig. 19) varies with respect to changes in the load. The decreasing trend of the voltage in this period is due to the gradual decrease in SOC (in Fig. 21). The discharge efficiency (in Fig. 21) varies between 0.6 and 0.75 depending on the load levels. At 04:00, the SOC reaches the lower threshold of 0.35, at which point the load is transferred to the grid.
- *Period 2* is from 04:00 to 11:00 when the load is served by the grid. Note that at approximately 06:00, PV power becomes available. From 04:00 to 06:00, the VRB is running on standby mode, which increases its voltage but lowers the efficiency significantly. From 06:00 to 09:00, the VRB is charged in bulk mode by the available power from PV arrays. During the bulk mode, the VRB charging current (in Fig. 20) tracks the PV output current and the voltage (in Fig. 19) increases rapidly. Once the voltage hits the absorb set point of 56.5 V at 09:00, it is held constant while the current

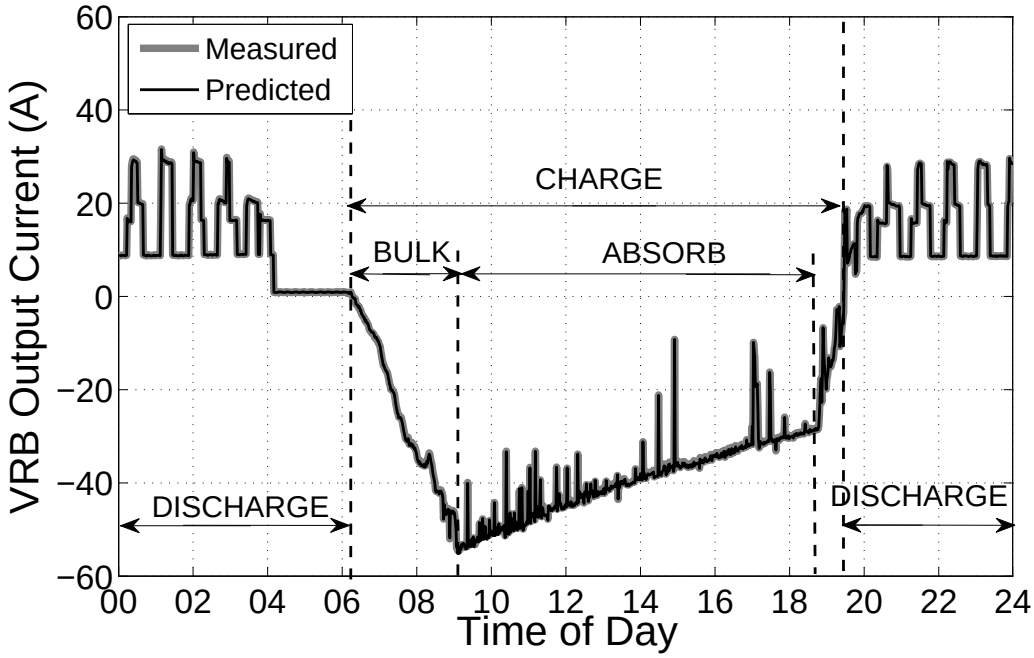

Fig. 20: VRB output current on 7 May 2013

slowly decreases

- *Period 3* is from 11:00 to 12:00 when the load is served by the renewable system again. From 11:00 to 19:00, the PV power is sufficient to simultaneously charge the VRB and serve the load. During this period, the charging efficiency is at its maximum because the VRB is charged at its maximum rate. After 19:00, the VRBs SOC is high enough to discharge when there is no PV power.

The actual and predicted system performance of May 2013 are given in Tab. II.

In Tab. II, the renewable system efficiency is the ratio between the renewable part of load energy and the PV energy taken by the system. Note from Fig. 18 that far more power is available from the PV system than is being utilized and that the PV utilization factor is 42% which indicates that the PV system is too large for the load and storage system. The system efficiency can be improved by serving a larger load, because at higher load the VRB is more efficient and also more direct PV power can be used. The time in Grid mode could also be reduced with a larger storage system.

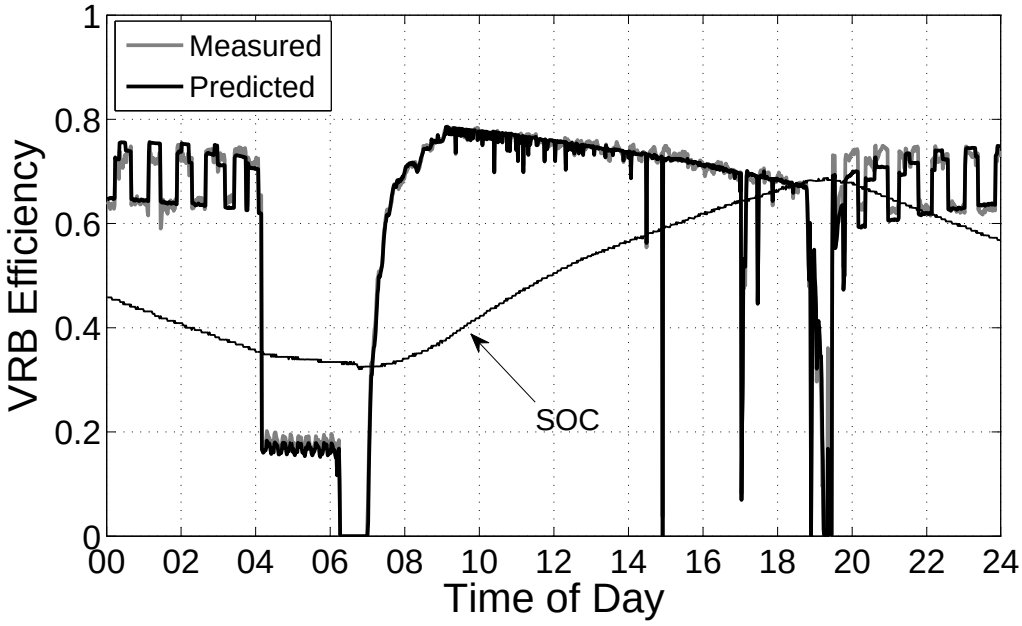

Fig. 21: VRB efficiency on 7 May 2013

V. VRB GENERALIZED PER-UNIT MODEL

VRB systems in practice are highly scalable due to the fact that high-power and high-capacity VRB systems are normally built by integrating a number of small standardized VRB modules of which power and capacity are determined by the number of cells

TABLE II: Microgrid System Performance in May 2013

	Actual (kWh)	Predicted (kWh)
Available PV energy	1857	–
PV energy taken by the system	787	805
Energy consumed by the load	493	–
Energy provided by the grid	145	143
VRB internal loss	43	45
VRB parasitic loss	198	202
HVAC loss	58	70
PV utilization factor	42%	43%
Renewable system efficiency	51.65%	50.55%

and the size of electrolyte tanks. Therefore, VRB system models should also be scalable. Therefore, the results in Section IV are generalized by converting the models from absolute to per-unit values.

A. Per-unit Model

Per-unit discharge and charge model are determined with the base values chosen as the rated voltage V_r and rated power P_r of the VRB module. All model coefficients are given in Tab.III

1) Discharge model: From (11), (13) and (15), open-circuit voltage, stack voltage and stack power are converted to per-unit as follow:

$$V_{oc}(p.u) = a_v^o TSOC + b_v^o T + c_v^o \tag{38}$$

$$V_{stack}^d(p.u) = a_v^d P_{load}(p.u) + b_v^d SOC + c_v^d \tag{39}$$

$$P_{stack}^d(p.u) = a_p^d P_{load}(p.u) + b_p^d SOC(SOC-1) + c_p^d \tag{40}$$

The efficiencies in (21) and (22) can be derived as:

$$\eta_d^v = \frac{a_v^d P_{load}(p.u) + b_v^d SOC + c_v^d}{a_v^o TSOC + b_v^o T + c_v^o} \tag{41}$$

$$\eta_d^p = \frac{P_{load}(p.u)}{a_p^d P_{load}(p.u) + b_p^d SOC(SOC-1) + c_p^d} \tag{42}$$

2) Charge model: From (26) and (30), stack voltage and stack power can be specified in per-unit as follow:

$$V_{stack}^c(p.u) = (a_v^c SOC + b_v^c) P_{charge}(p.u) + c_v^c SOC + d_v^c \tag{43}$$

$$P_{stack}^c(p.u) = (a_p^c SOC + b_p^c) P_{charge}(p.u) + c_p^c SOC + d_p^c \tag{44}$$

The efficiencies in (33) and (34) can be determined as:

$$\eta_c^v = \frac{a_v^o TSOC + b_v^o T + c_v^o}{(a_v^c SOC + b_v^c) P_{charge}(p.u) + c_v^c SOC + d_v^c} \tag{45}$$

$$\eta_c^p = \frac{(a_p^c SOC + b_p^c) P_{charge}(p.u) + c_p^c SOC + d_p^c}{P_{charge}(p.u)} \tag{46}$$

TABLE III: VRB per-unit model coefficients

	a_k^i	b_k^i	c_k^i	d_k^i
$(i,k)=(o,v)$	$\frac{0.001N_c}{V_r}$	$\frac{-1.1755N_c}{V_r}$	$\frac{1.6123N_c}{V_r}$	–
$(i,k)=(d,v)$	$\frac{-2.72P_r}{V_r}$	$\frac{6.3606}{V_r}$	$\frac{47.335}{V_r}$	–
$(i,k)=(d,p)$	1.0334	$\frac{1.127}{P_r}$	$\frac{0.596}{P_r}$	–
$(i,k)=(c,v)$	$\frac{1.895P_r}{V_r}$	$\frac{1.552P_r}{V_r}$	$\frac{6.82}{V_r}$	$\frac{46.79}{V_r}$
$(i,k)=(c,p)$	-0.128	1.05	$\frac{0.19}{P_r}$	$\frac{-0.59}{P_r}$

B. Validity Domain of the Model

The experimental data presented in this paper were sampled every 5 s and averaged over a 1-min window, therefore the developed VRB model is valid when considering loads and changes in solar insolation that change in this time frame. Fast transients in load and switching operations may possibly lead to changes in efficiency due to heating or other effects that would not be captured in this model. For example, the effects of a load spike or isolated cloud cover may not be captured if these phenomena do not last longer than 5 s. Furthermore, this model has not been validated in extreme temperature ranges. Although the effect of the HVAC system was modeled, there may be additional aspects to consider during extremely hot or cold weather.

The models are valid regardless of whether the system is gridconnected or islanded. During islanded operation, the load would not be served during VRB stand-by mode and the efficiency of the system would be impacted. For an analysis of how the model may perform at different latitudes, the interested reader is referred to an earlier analysis that addresses some of these issues [8]

VI. CONCLUSIONS AND FUTURE WORK

In this paper, a PV-VRB microgrid system performance has been characterized. The system operating characteristics, losses, and efficiencies are quantified and formulated

based on measured data. The VRB discharge and charge efficiencies are found to be non-linear with the load/charge power. Based on the system characterization, a scalable model has been built to accurately predict the system behavior and performance. A case study has been performed for May 2013. The storage size is shown to be too small to utilize the available PV power. Future work in this area will include optimizing the size of the PV-VRB system to maximize the PV utilization and also in control strategies to maximize the efficiency of the system.

Acknowledgments

The authors gratefully acknowledge the financial support of the Army Corps of Engineers under contract W9132T-12-C-0016.

References

[1] J. Chahwan, C. Abbey, and G. Joos, "VRB modelling for the study of output terminal voltages, internal losses and performance," in *Electrical Power Conference, 2007. EPC 2007. IEEE Canada*, Oct. 2007, pp. 387 –392.

[2] T. Nguyen, X. Qiu, T. Gamage, M. L. Crow, B. McMillin, and A. C. Elmore, "Microgrid application with computer models and power management integrated using PSCAD/EMTDC," *Proc. North Amer. Power Symp.*, 2011.

[3] L. Barote, C. Marinescu, and M. Georgescu, "VRB modeling for storage in stand-alone wind energy systems," in *PowerTech, 2009 IEEE Bucharest*, July 2009.

[4] C. Blanc and A. Rufer, "Multiphysics and energetic modeling of a vanadium redox flow battery," in *IEEE 2008 International Conference on Sustainable Energy Technologies*, Nov. 2008, pp. 696 –701.

[5] M. Vijayakumar, L. Li, Z. Nie, Z. Yang, and J. Z. Hu, "Structure and stability of hexa-aqua v(iii) cations in vanadium redox flow battery electrolytes," *Physical Chemistry Chemical Physics*, vol. 14, 2010.

[6] M. Vijayakumar, L. Li, G. Graff, J. Liu, H. Zhang, Z. Yang, and J. Z. Hu, "Towards understanding the poor thermal stability of v5+ electrolyte solution in vanadium redox flow batteries," *Journal of Power Sources*, vol. 196, no. 7, pp. 3669 – 3672, 2011.

[7] X. Ma, H. Zhang, C. Sun, Y. Zou, and T. Zhang, "An optimal strategy of electrolyte flow rate for vanadium redox flow battery," *Journal of Power Sources*, vol. 203, pp. 153 – 158, 2012.

[8] J. Guggenberger, A. C. Elmore, J. Tichenor, and M. L. Crow, "Performance prediction of a vanadium redox battery for use in portable, scalable microgrids," *IEEE Transactions on Smart Grid*, vol. 3, no. 4, 2012.

[9] M. Li and T. Hikihara, "A coupled dynamical model of redox flow battery based on chemical reaction, fluid flow, and electrical circuit," *IEICE Transactions*, vol. 91-A, no. 7, pp. 1741–1747, 2008.

[10] K. Knehr and E. Kumbur, "Open circuit voltage of vanadium redox flow batteries: Discrepancy between models and experiments," *Electrochemistry Communications*, vol. 13, no. 4, pp. 342 – 345, 2011.

II. OPTIMAL SIZING OF A VANADIDUM REDOX BATTERY SYSTEM FOR MICROGRID SYSTEMS

Tu A. Nguyen, M. L. Crow, *IEEE Fellow*, and A. C. Elmore*

Department of Electrical and Computer Engineering

*Department of Geological Engineering

Missouri University of Science and Technology, Rolla, MO 65401

Abstract

The vanadium redox battery (VRB) has proven to be a reliable and highly-efficient energy storage system for microgrid applications. However, one challenge in designing a migrogrid system is specifying the size of the energy storage system. This selection is made more complex due to the independent power and energy ratings inherent in VRB systems. Sizing a VRB for both required power output and energy storage capacity requires an in-depth analysis to produce both optimal scheduling capabilities and minimum capital costs. This paper presents an analytical method to determine the optimal ratings of VRB energy storage based on an optimal scheduling analysis and cost-benefit analysis for microgrid applications. A dynamic programming algorithm is used to solve the optimal scheduling problem considering the efficiency and operating characteristics of the VRBs. The proposed method has been applied to determine the optimal VRB power and energy ratings for both isolated and grid-connected microgrids which contain PV arrays and fossil-fuel-based generation. We first consider the case in which a grid-tie is not available and diesel generation is the backup source of power. The method is then extended to consider the case in which a utility grid tie is available.

Index Terms

Microgrids, renewable energy, energy storage, vanadium redox battery, optimal scheduling, optimal sizing

I. INTRODUCTION

The integration of renewable energy resources in microgrids has been increasing in the recent decades. Higher penetration of renewable energy is an environmentally-friendly solution for improving the reliability and decreasing costs of microgrid systems. Renewable power sources are typically highly variable depending on weather conditions, thereby necessitating the use of highly-efficient and rapid response energy storage systems (ESS) to store the surplus renewable energy and re-dispatch that energy when needed. One of the most recent ESS technologies commercially available is the vanadium redox battery (VRB). The VRB exhibits many advantages over many traditional battery storage systems; the VRB has independent power and energy ratings, quick charge and discharge response, high efficiency, long life cycle, low self-discharge, and an easily estimated state of charge. By proper control and scheduling of the VRB system, the microgrid operating costs can be significantly reduced. However, the initial capital and maintenance costs for the VRB are still relatively high in comparison to other energy storage systems (such as lead acid batteries) [1]. Therefore it is imperative to size and operate the VRB such that the reduction in operating costs can justify the increase in the capital investment. In this paper, the operating cost can be characterized as a function of VRB ratings (both power and energy) to better quantify the cost-benefit analyses.

Although a number of studies have been conducted on the ESS sizing problem for microgrids, most work has focused on lead-acid or Li-on batteries [2–5]. In [6], the relationship between the ESS capacity and daily operating cost is found by solving the unit commitment problem for the microgrid. In [1], the problem is similarly solved with additional reliability constraints. The cost analysis to determine the optimal size of a compressed-air storage system for large scale wind farms was introduced in [7]. The cost sensitivity of varying ESS sizes and technologies for wind-diesel systems was analyzed in [8]. However, in these previous analyses, the ESS charge and discharge efficiencies were often neglected or considered as constants, furthermore the charging limit of the batteries under different conditions of the state of charge (SOC) and charging voltage

was not considered. We extend these earlier works to include these oversights.

As opposed to other ESS, the VRB's charge/discharge efficiencies can be characterized as explicit non-linear functions of charge/discharge power and the SOC [9]. Furthermore, the VRB's power and energy ratings are independently scalable, which allows better flexibility in sizing the VRB for microgrid systems. Therefore, this paper focuses on the optimal sizing of power and energy ratings for a VRB system in isolated and grid-connected microgrids. An analytical method is developed to solve the problem based on a per-day cost model in which the operating cost is obtained from optimal scheduling. The charge, discharge efficiencies, and operating characteristics of the VRB are considered in the problem. Case studies are performed under different conditions of load and solar insolation.

II. FORMULATION OF THE OPTIMAL SIZING PROBLEM FOR VRB MICROGRIDS

A. Problem Definition

In this paper, the optimal size of the VRB is defined as the independent power and the energy ratings required to minimize the total cost per day. The cost per day is determined by:

$$TC = TCPD + OC - TB \tag{1}$$

where $TCPD$ is the total capital cost amortized per day for the VRB, OC is the total operating cost of the system in that day, and TB is the total benefit achieved by selling the extra renewable energy to the grid. If isolated microgrids are considered, then TB is zero.

The following data are given as inputs to the formulation:

- Maximum and minimum load power,
- Power rating of the PV arrays and the diesel generators,
- Historical hourly insolation profile for the site,

- Buying and selling prices of the utility's electricity.

The system constraints are:

- *R1: The primary system load will always be met.* This ensures that the high priority (primary) loads of the system are always served. The primary loads have been identified prior to microgrid deployment.
- *R2: Sufficient energy capacity will always be held in reserve to meet essential load demand if fuel becomes unavailable.* This constraint ensures that if the fuel supply is compromised (through disaster, inclement weather, etc.), there is enough energy reserve to serve the primary load for a pre-specified length of time (typically between 1 hour and 36 hours).
- *R3: The VRB is not charged (or discharged) beyond the maximum (or minimum) recommended efficiency and/or operational SOC limits.* To achieve optimal performance, the VRB is not allowed to operate if its efficiency drops below a predetermined threshold.
- *R4: The charging rate is limited by the absorb power*. The charging rate of the VRB is limited by electrochemical processes which depend on both the VRB SOC and the voltage. This constraint ensures that the charging rate conforms to physical limitations.
- *R5: The VRB is charged only by the PV array.* One of the primary objectives of a microgrid is to minimize the amount of fossil fuel used, therefore the VRB may only be charged via renewable resources and not by the diesel generator or the utility grid tie.
- *R6: The diesel generator is not operated at light load.* The diesel generators are most efficient when heavily loaded, therefore it is preferred to run fewer generators at higher output.
- *R7: Once a generator is started (or shut down) it remains online (or offline) a minimum time before changing its status.* This constraint minimizes "chopping" (discontinuous operation) around breakpoints.

B. Per-day Cost Model

1) Capital cost: The total capital of an ESS includes a one-time investment and the annual maintenance cost [6]. The annual financial requirement of the VRB is calculated as [10]:

$$AC = c_i TI + P_{vrb}^{rated} OM \tag{2}$$

$$TI = c_p P_{vrb}^{rated} + c_e E_{vrb}^{rated} + c_o \tag{3}$$

where

- AC is annualized capital ($\$/yr$),
- TI is the one-time investment ($\$$),
- $c_i = \frac{i(1+i)^l}{(1+i)^l - 1}$ is the annual carrying charge factor (equal to 0.162 with typical 10-year life cycle and a 10% interest rate),
- OM is the fixed operation and maintenance cost ($\$/kWyr$),
- c_p is the power related cost ($\$/kW$),
- c_e is the energy related cost ($\$/kWh$),
- P_{vrb}^{rated} is the power rating of the VRB (kW),
- E_{vrb}^{rated} is the energy rating of the VRB (kWh),
- c_o is the fixed cost (accounts for structure, housing, and installation costs) ($\$$).

The total capital cost of the VRB system per day is therefore:

$$\begin{aligned} TCPD &= \frac{AC}{365} \\ &= \frac{(c_i c_p + OM) P_{VRB} + c_i c_e E_{VRB} + c_i c_o}{365} \end{aligned} \tag{4}$$

In [11], the cost information is given for VRB energy storage systems with power ratings ranging from $200kW$ to $10MW$ and with durations from 2 to 16 hours. These costs are: $OM = 58.4\$/kWyr$, $c_p = 2300\$/kW$, $c_e = 300\$/kWh$ and $c_o = \$250,000$. For smaller scale VRB systems, c_p and c_e are still in the same range, however c_o is

smaller due to the smaller structure, housing, and installation costs. In this paper, c_o is estimated to be $\$25,000$ for a $10kW$-scale system (Fig. 1).

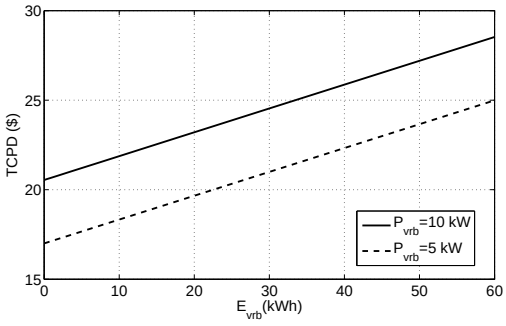

Fig. 1: Total capital cost per day for a 10kW-scale system

2) Operating cost: For an isolated PV-diesel microgrid, the operating cost is the daily fuel cost of the diesel generators. For a grid-connected microgrid, the operating cost is the sum of the diesel fuel costs and the cost of the grid electricity. The expected operating cost can be determined:

- For an isolated microgrid:

$$OC = \sum_{k=1}^{N} \left[\sum_{i=1}^{m} C_{dgi} H_{dgi}(P_{dgi,k}) T \right] \tag{5}$$

- For a grid-connected microgrid:

$$OC = \sum_{k=1}^{N} \left[\sum_{i=1}^{m} C_{dgi} H_{dgi}(P_{dgi,k}) T + C_{buy,k} P_{grid,k} T \right] \tag{6}$$

where

- N is the number of time periods in a one day cycle,
- T is duration of each time period,
- m is the number of diesel generators,
- $H_{dgi}(gal/h)$, which is a function of $P_{dgi,k}$, is the fuel consumption of diesel generator i,
- $C_{dgi}(\$/gal)$ is the fuel price for diesel generator i,

- $C_{buy,k}(\$/kWh)$ is the electricity buying price in time period k,
- $P_{dgi,k}$ is the dispatched power for diesel generator i in time period k, and
- $P_{grid,k}$ is the power supplied by the grid in time period k.

3) Benefit: For a grid-connected microgrid, the unused renewable power can be sold to the grid as a benefit. The total benefit per day is then:

- For an isolated microgrid:

$$TB = 0 \tag{7}$$

- For a grid-connected microgrid:

$$TB = \sum_{k=1}^{N} C_{sell,k} P_{ext,k} T \tag{8}$$

in which

- $C_{sell,k}(\$/kWh)$ is the electricity selling price in time period k, and
- $P_{extra,k}$ is the power sold to the grid in time period k.

C. Problem Formulation

From equations (4) and (6), the objective function is:

$$\min(TC) = \min(TCPD + OC - TB) \tag{9}$$

where the constraints are expressed as:

$R1$: $\sum_{i=1}^{m} P_{dgi,k} + P_{vrb,k} = P_{load,k} - P_{PV,k}$

$R2$: $SOC_{vrb,k} E_{vrb} \geq E_{resv}$

$R3$: $SOC_{vrb}^{min} \leq SOC_{vrb,k} \leq SOC_{vrb}^{max}$

$R4$: $P_{vrb,k} \leq P_{ab,k}(SOC_{vrb,k}, V_{ab,k})$

$R5$: $P_{vrb,k} \geq 0$ if $P_{dg,k} > 0$

$R6$: $P_{dgi}^{min} \leq P_{dgi,k} \leq P_{dgi}^{max}$

$R7$:
$$\begin{cases} T_{dgi,k}^{up} \geq T_{dgi}^{up,min} & \text{if generator } i \text{ is online} \\ T_{dgi,k}^{dw} \geq T_{dgi}^{dw,min} & \text{if generator } i \text{ is offline} \end{cases}$$

in which

- $P_{load,k}$ is the demand in period k,
- $P_{PV,k}$ is power output of PV arrays in period k,
- $P_{vrb,k}$ is the dispatched power for VRB in period k, where $P_{vrb,k} \geq 0$ if the VRB is discharging and $P_{vrb,k} < 0$ if the VRB is charging,
- $SOC_{vrb,k}$ is the state of charge of VRB in period k,
- E_{vrb} is the capacity rating of the VRB,
- E_{resv} is the energy reserve requirement for storage,
- SOC_{vrb}^{min} and SOC_{vrb}^{max} are the highest and lowest allowable state of charge respectively,
- $P_{ab,k}$ and $V_{ab,k}$ are the absorb power and absorb voltage of the VRB in period k respectively,
- P_{dgi}^{min} and P_{dgi}^{min} are the power output limits of diesel generator i, and
- $T_{dgi,k}^{up/dw}$ is the up/down time of diesel generator i until period k, where $T_{dgi}^{up/dw,min}$ is the minimum up/down time for diesel generator i.

III. MICROGRID COMPONENT CHARACTERIZATION

To operate the system at greatest efficiency, each of the system components must be characterized with respect to their power and energy consumption versus efficiencies. These characteristics will be integrated into the objective function (9) and constraints *R1-R7*.

A. PV Array

Assuming that maximum power point tracking is used, the output power of the PV array can be calculated:

$$P_{PV} = P_{max,STC} I_s + 0.001(T_c - 25)K_p \tag{10}$$

where

- $P_{max,STC}$ (in kW) is the maximum power at the standard operating condition ($1kW/m^2$, 25^oC),
- I_s (in kW/m^2) is the solar insolation,
- T_c (in ^oC) is the panel temperature,
- K_p (in $W/^oC$) is the sensitivity of the output power to temperature.

The panel temperature can be found from the ambient temperature by:

$$T_c = \frac{NOCT - 25}{0.8} I_s + T_a \tag{11}$$

where $NOCT$ is the normal operating cell temperature measured at $0.8kW/m^2$ and 20^oC.

All of the coefficients and parameters can be obtained from manufacturers' data or by experimental characterization.

B. Diesel Generator

The fuel consumption of a diesel generator can be characterized as a linear function of output power [12]:

$$H_{dg}(P_{dg}) = B_{dg} P_{dg}^{rated} + A_{dg} P_{dg} \tag{12}$$

where H_{dg} is the fuel consumption in gal/hr, P_{dg}^{rated} and P_{dg} are the rated power and output power of the diesel generator in kW respectively, and A_{dg} and B_{dg} are the coefficients of the consumption curve in gal/kWh.

The efficiency η_{dg} in $\%$ of diesel generator output is calculated based on the fuel consumption function [13]:

$$\eta_{dg} = \frac{100 P_{dg}}{H_{dg} LHV_{gas}} \tag{13}$$

where LHV_{gas} is the lower heating value of the fuel in kWh/gal, which for diesel fuel is $LHV_{dg} = 43.75\ kWh/gal$.

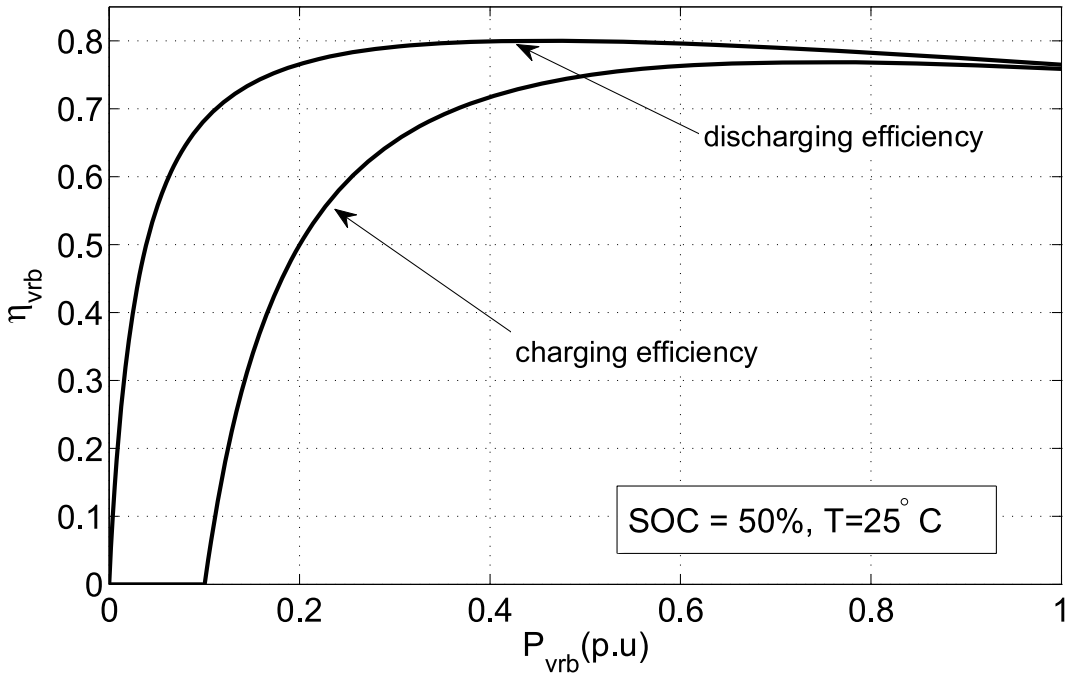

Fig. 2: VRB charge and discharge efficiencies

C. VRB

$SOC_{vrb,k}$ is the state of charge of VRB in period k, such that

$$SOC_k = \begin{cases} SOC_{k-1} - \frac{P_{vrb,k}T}{\eta^d_{vrb}E_{vrb}} & \text{if discharging} \\ SOC_{k-1} - \frac{P_{vrb,k}\eta^c_{vrb}T}{E_{vrb}} & \text{if charging} \end{cases} \tag{14}$$

Note that the VRB SOC is a function of power, energy, and efficiency, where η^d_{vrb} and η^d_{vrb} are the discharge and charge efficiencies, respectively.

The per-unit discharge and charge models are developed in [9]. During discharge, the discharge efficiency is:

$$\eta^d_{vrb} = \eta^d_v \eta^d_p \tag{15}$$

where

$$\eta_v^d = \frac{a_v^d P_{vrb}(p.u.) + b_v^d SOC + c_v^d}{a_v^o T_e SOC + b_v^o T_e + c_v^o} \tag{16}$$

$$\eta_p^d = \frac{P_{vrb}(p.u.)}{a_p^d P_{vrb}(p.u.) + b_p^d SOC(SOC-1) + c_p^d} \tag{17}$$

and η_v and η_p^d are respectively the voltage and stack efficiencies and T_e is the electrolyte temperature in K^o.

During charge, the VRB efficiency is:

$$\eta_{vrb}^c = \eta_v^c \eta_p^c \tag{18}$$

where

$$\eta_v^c = \frac{a_v^o T_e SOC + b_v^o T_e + c_v^o}{(a_v^c SOC + b_v^c) P_{vrb}(p.u.) + c_v^c SOC + d_v^c} \tag{19}$$

$$\eta_p^c = \frac{(a_p^c SOC + b_p^c) P_{vrb}(p.u.) + c_p^c SOC + d_p^c}{P_{vrb}(p.u.)} \tag{20}$$

The absorb power is the maximum power that the VRB can absorb during charging when the voltage is regulated to be constant. It is characterized as a function of absorb voltage and the SOC:

$$P_{ab}(p.u.) = (a_{ab} V_{ab}(p.u.) + b_{ab}) SOC + c_{ab} V_{ab}(p.u.) + d_{ab} \tag{21}$$

All model coefficients are given in Table I and the charge and discharge efficiencies as a function of power are shown in Fig. 2.

IV. ANALYTICAL APPROACH

In eq. (4), the total cost per day (TCPD) of the VRB has been characterized as an explicit function of power (P_{vrb}^{rated}) and energy (E_{vrb}^{rated}) ratings. At specific values of P_{vrb}^{rated} and E_{vrb}^{rated}, the TCPD is constant and independent of the operating cost and the total benefit of the microgrid. Therefore, the process of minimizing TC becomes the minimization of $(OC - TB)$ by finding an optimum dispatch pattern for the generators,

TABLE I: VRB per-unit model coefficients

(i,k)	a_k^i	b_k^i	c_k^i	d_k^i
(o,v)	0.07917	-0.00244	1.27640	–
(d,v)	-0.28333	0.13251	0.98614	–
(d,p)	1.0334	0.34540	0.1192	–
(c,v)	0.19739	0.16167	0.14208	0.97479
(c,p)	-0.128	1.05	0.038	0.118
(a,b)	-8.3904	8.6634	7.3632	-7.504

the grid-tie, and the VRB as a function of PV power output. However, assuming constant power and energy ratings provides only a local optimal solution. To obtain the global solution for the optimization, the optimization should be performed over the whole domain of P_{vrb}^{rated} and E_{vrb}^{rated}. The existence of a solution for an optimal VRB size is guaranteed in this problem due to the fact that the TCPD is linearly increasing whereas the operating cost is decreasing when P_{vrb}^{rated} and E_{vrb}^{rated} are increasing, resulting in a convex optimization surface.

Fig. 3 shows a flowchart of the algorithm to search for optimal size of the VRB. The algorithm contains the following main steps:

A. Domain Definition

As previously mentioned, P_{vrb}^{rated} and E_{vrb}^{rated} are independent, which means the search domain is a multi-multidimensional space. To narrow the search space, upper and lower limits of P_{vrb}^{rated} and E_{vrb}^{rated} are defined:

$$\begin{cases} P_{vrb}^{rated,min} \leq P_{vrb}^{rated} \leq P_{vrb}^{rated,max} \\ E_{vrb}^{rated,min} \leq E_{vrb}^{rated} \leq E_{vrb}^{rated,max} \end{cases}$$

Due to the constraint that requires the energy storage to serve a critical load during

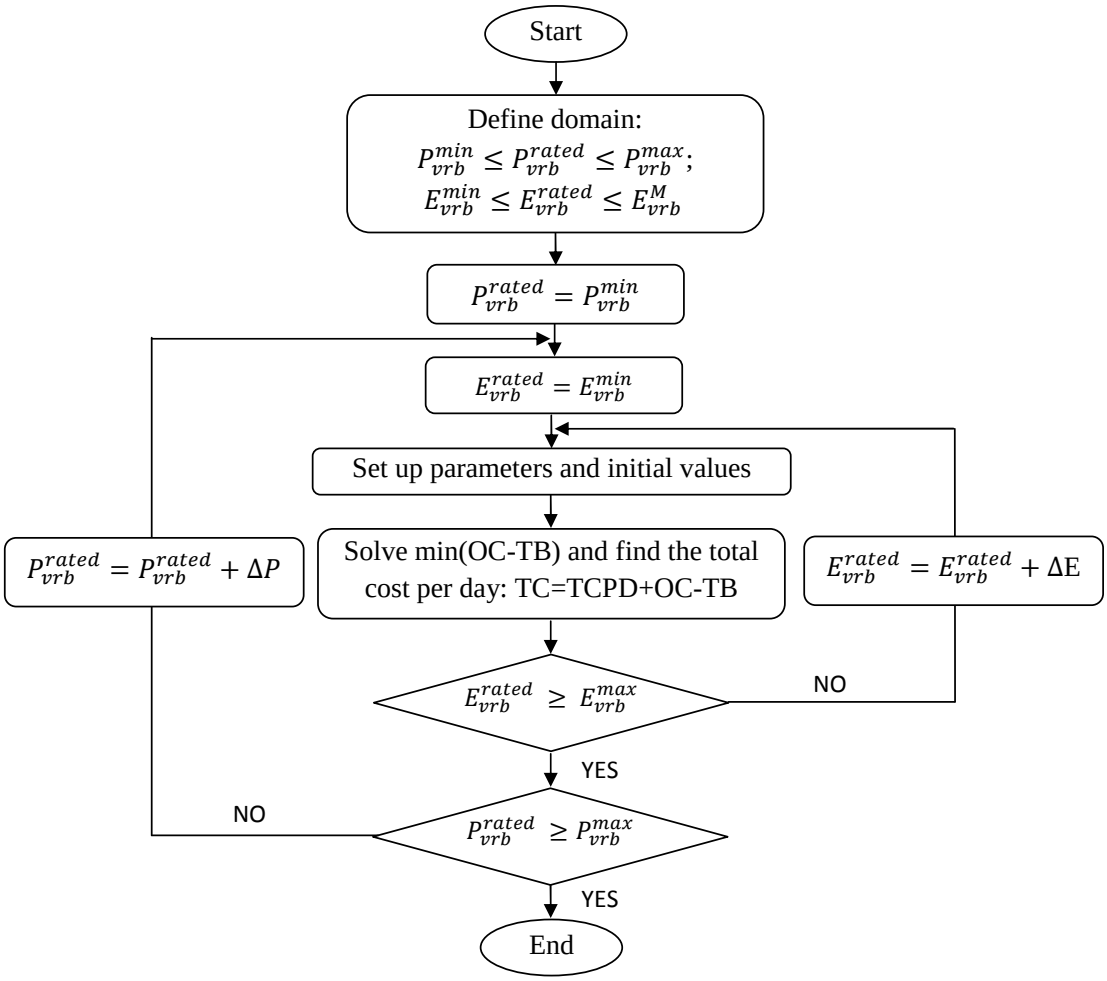

Fig. 3: VRB optimal size search flow chart

a minimum period of time when the fuel is not available, $E_{vrb}^{rated,min}$ is defined as the minimum required reserve. $P_{vrb}^{rated,min}$ is chosen as the maximum of the priority loads. In this problem, it is assumed that renewable power is available to charge the VRB only if the PV power is greater than the load power. Therefore, $P_{vrb}^{rated,max}$ and $E_{vrb}^{rated,max}$ can be specified:

$$P_{vrb}^{rated,max} = P_{PV}^{rated} - P_{load}^{min} \tag{22}$$

$$E_{vrb}^{rated,max} = P_{PV}^{rated} T_{peak} - N P_{load}^{min} \tag{23}$$

where P_{PV}^{rated} and P_{load}^{min} are the rated PV power and the daily minimum load respectively and T_{peak} is the time (in hours) at which the daily insolation is a maximum. N is the number of time increments per day over which the optimization occurs (typically 24 hours).

B. The Optimization Algorithm

From the solar insolation, the available PV output power is calculated from eq. (10). At a specific P_{vrb}^{rate} and E_{vrb}^{rated}, the optimal operation scheduling problem is set up with objective function (9) and the constraints as determined by ***R1-R8***. The problem is solved by Dynamic Programming (DP) as proposed in [14]. The main advantage of DP is it can maintain solution feasibility by its ability to find the optimum sub-sequence while searching for the optimum sequence. Dynamic programming can be computationally burdensome. For example, in an N-unit system, there are $2^N - 1$ combinations at each period and for M periods the total number of combinations is $(2^N - 1)^M$. For a large scale system the computation required to traverse this space can be overwhelming. However, in microgrid applications, the small number of units and large number of constraints significantly decrease the search space, therefore dynamic programming can be an appropriate choice of algorithm.

The solution of the optimal scheduling problem provides the minimum value of $(OC - TB)$ and the loading pattern for the microgrid. The total cost per day is also found from eq. (1). At a constant value P_{vrb}^{rated}, characterizing the relationship between total cost per day and the energy rating provides a suboptimal solution. The process is repeated with increasing incremental values of P_{vrb}^{rated} until the upper limit is reached. The optimal solution is then obtained as the minimum value of the suboptimal solutions.

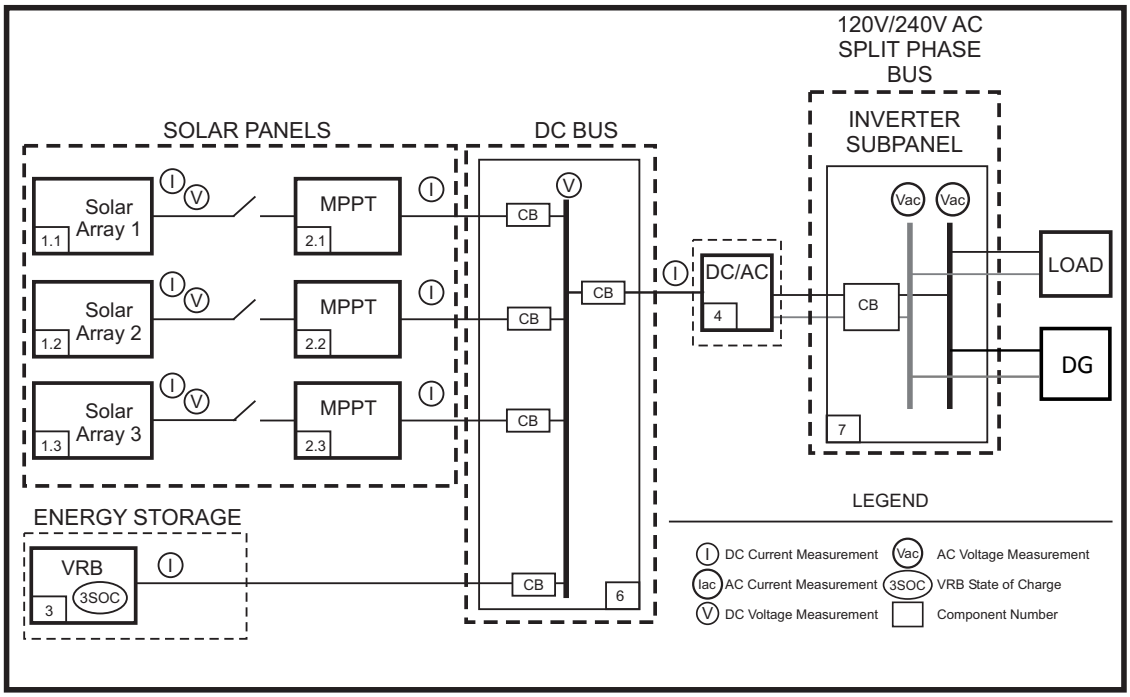

Fig. 4: PV-Diesel Microgrid Oneline Diagram

V. CASE STUDIES RESULTS

The case studies are performed to illustrate the optimization method. These cases are based on an actual microgrid system located at the Fort Leonard Wood US Army base in Missouri, USA (Fig. 4), which can be either isolated or grid-connected. The AC load ranges between 2-5 kW. The PV arrays are rated 15 kW. Hourly data of the solar insolation and ambient temperature at the site were collected from December 2012 to September 2013. The diesel generator (DG) maximum output is 8 kW. The initial state and fuel consumption of the DG are given in Table II. Fuel usage at forward operating military bases will vary with size, location, and mission. By the time fuel reaches in-theater staging, it can cost 10 or more times the domestic price [15]. Similarly, fuel costs in extreme rural areas experience significant inflation due to transportation costs. For example, delivering fuel to rural areas of Alaska is complicated and expensive, since fuel must typically be delivered by either barge or plane [16]. Electricity price will also vary

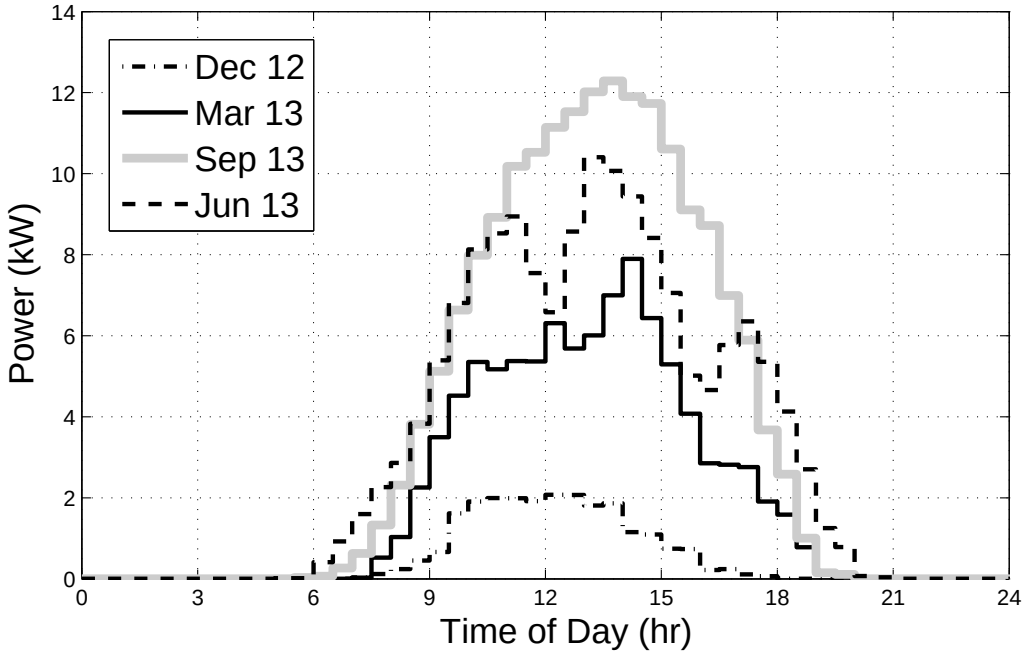

Fig. 5: PV output power data

widely with locations. The electricity in the remote areas can cost double or more the price in urban cities due to the high cost of transmission and generation. For example, the average electricity price for residential customers in Hawaii in June 2014 is ¢38.66/kWh [17]. Therefore, to better approximate the deployed performance of the microgrid, a diesel fuel cost of $40/gal, electricity price of ¢40/kWh and buy back price of ¢20/kWh were used in this study.

TABLE II: Diesel generator data

A_{dg}	B_{dg}	Initial state
0.065 gal/kWh	0.0215 gal/kWh	2 hr
$T_{dg}^{up,min}$	$T_{dg}^{dw,min}$	Fuel cost
1 hr	1 hr	$40/gal

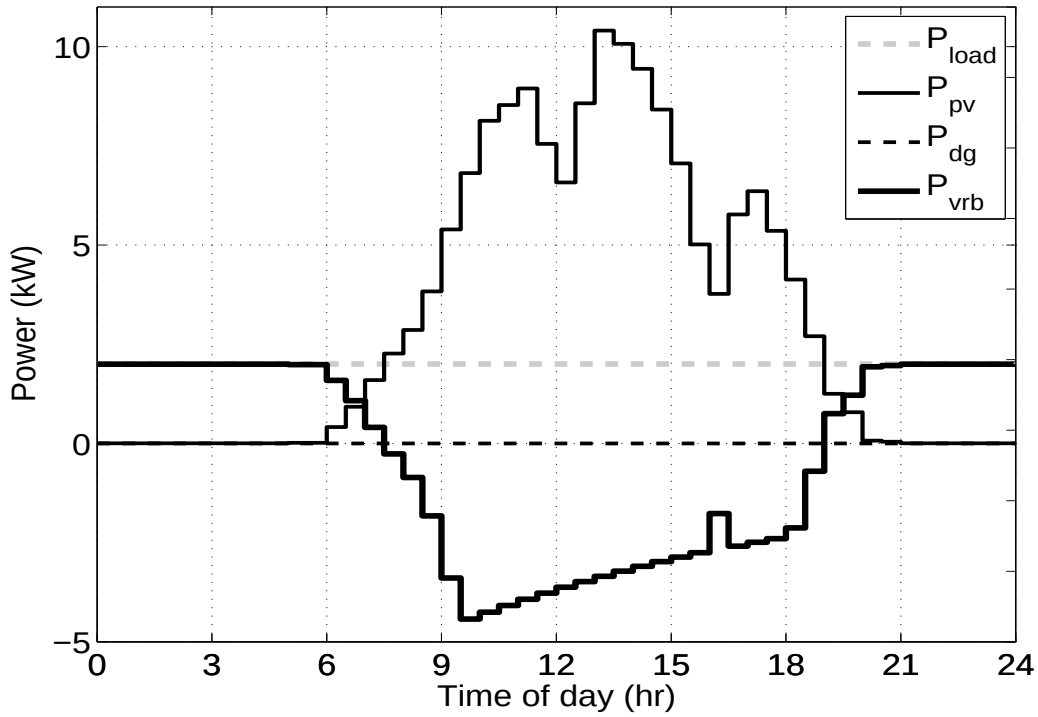

Fig. 6: Dispatch on one day of June 2013 at minimum load and $P_{VRB}^{rated} = 5$ kW and $E_{VRB}^{rated} = 65$ kWh

The energy storage is required to have a reserve of 2 kWh, which is sufficient to run the minimum critical load for 1 hour. The VRB may discharge to a SOC of 20%. The VRB is assumed to be initialized at the minimum 20% SOC at the beginning of the day (12am). The VRB rating range considered is

$$5kW \leq \quad P_{vrb}^{rated} \quad \leq 10kW$$

$$10kWh \leq \quad E_{vrb}^{rated} \quad \leq 100kWh$$

The optimization is solved using PV data from four days in December 2012, March 2013, June 2013, and September 2013 (Fig. 5) which represent typical scenarios of solar insolation ranging from a low in December 2012 to a high in September 2013. From the given weather data, the PV power output is calculated from eq. (10) for both

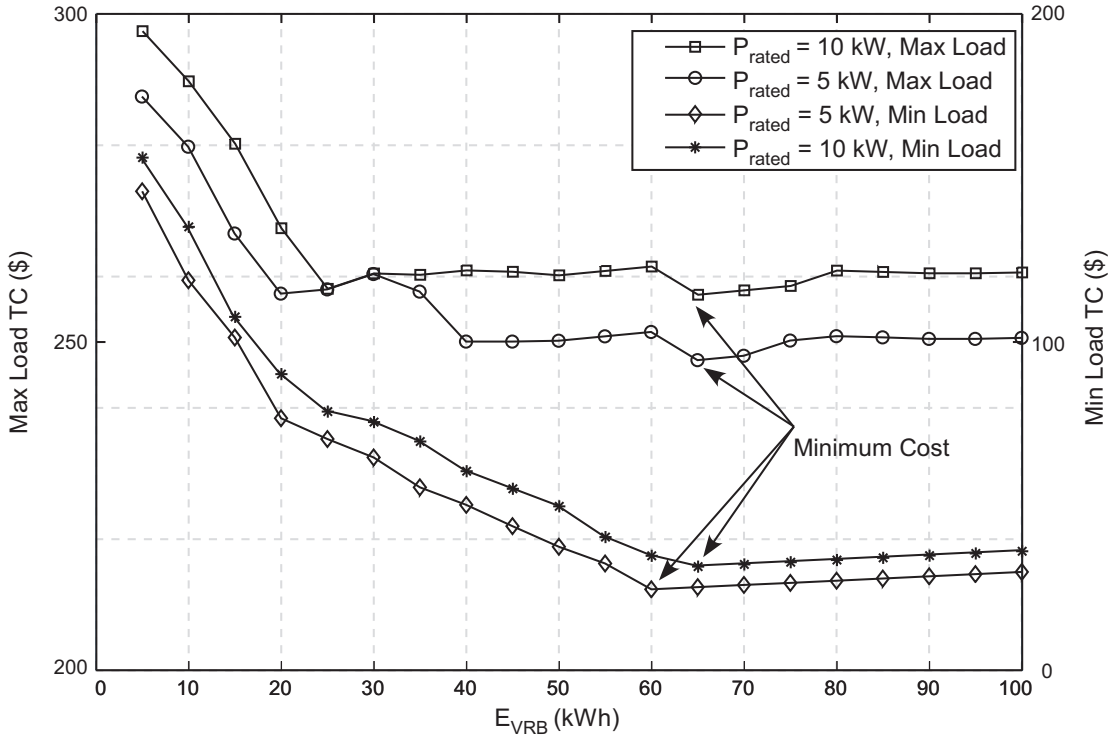

Fig. 7: Costs for operation in June 2013 at minimum and maximum load for a power rating P_{vrb}^{rated} of 5 kW and 10 kW

the minimum and maximum system loads. The optimization process illustrated in Fig. 3 is used to find the optimal size of the VRB for both maximum load and minimum load scenarios for both isolated and grid-connected cases.

A. Case Study I - Isolated Microgrid

In this case study, the microgrid is isolated and the load must be met through the combination of PV, diesel generation, and VRB energy storage. The optimization process yields a series of operating scenarios that have associated costs. As an example of these, the costs for the minimum and maximum load cases for June 2013 are shown in Fig. 7 for both power ratings. Note that the cost axis for minimum load is on the right side of the figure and the maximum load cost is on the left axis. There is not a single combination of power and energy ratings that provides a consistent minimum, but there

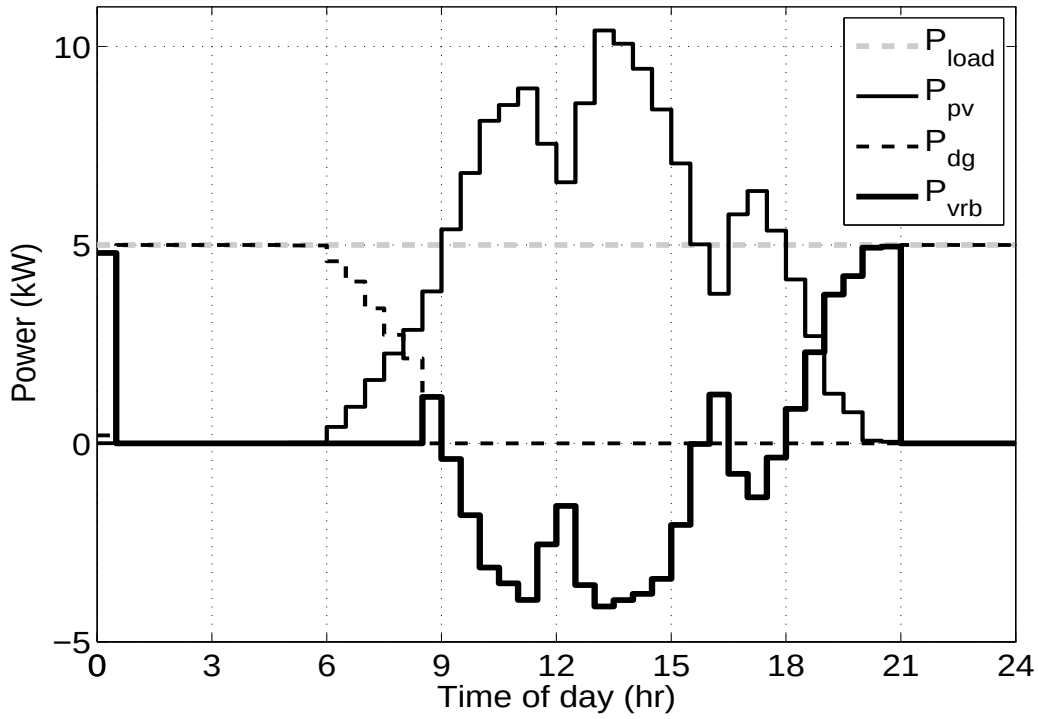

Fig. 8: Dispatch on one day of June 2013 at maximum load and $P_{VRB}^{rated} = 5$ kW and $E_{VRB}^{rated} = 65$ kWh

is definitely commonality between the traces. Note that the minimum cost occurs at a 65 kWh VRB rating except in the 5kW VRB minimum load case, in which the minimum occurs at 60 kWh rating. However, the minimum costs between the 65 kWh and 60 kWh ratings are very close.

Figures 6 and 8 show the operating profiles of the (5 kW, 65 kWh) rated VRB for June 2013 under minimum and maximum loads respectively. In the minimum load case, the diesel generator never engages which is why the operating costs are much smaller than for the maximum load case. In the maximum load case the diesel generator runs at night, but note that it ramps down as the sunlight increases. Also note that when the diesel hits the minimum limit (35% loading) at just before 09:00 it is disengaged and the VRB picks up the load in correspondence with Constraint R6. The VRB also picks up

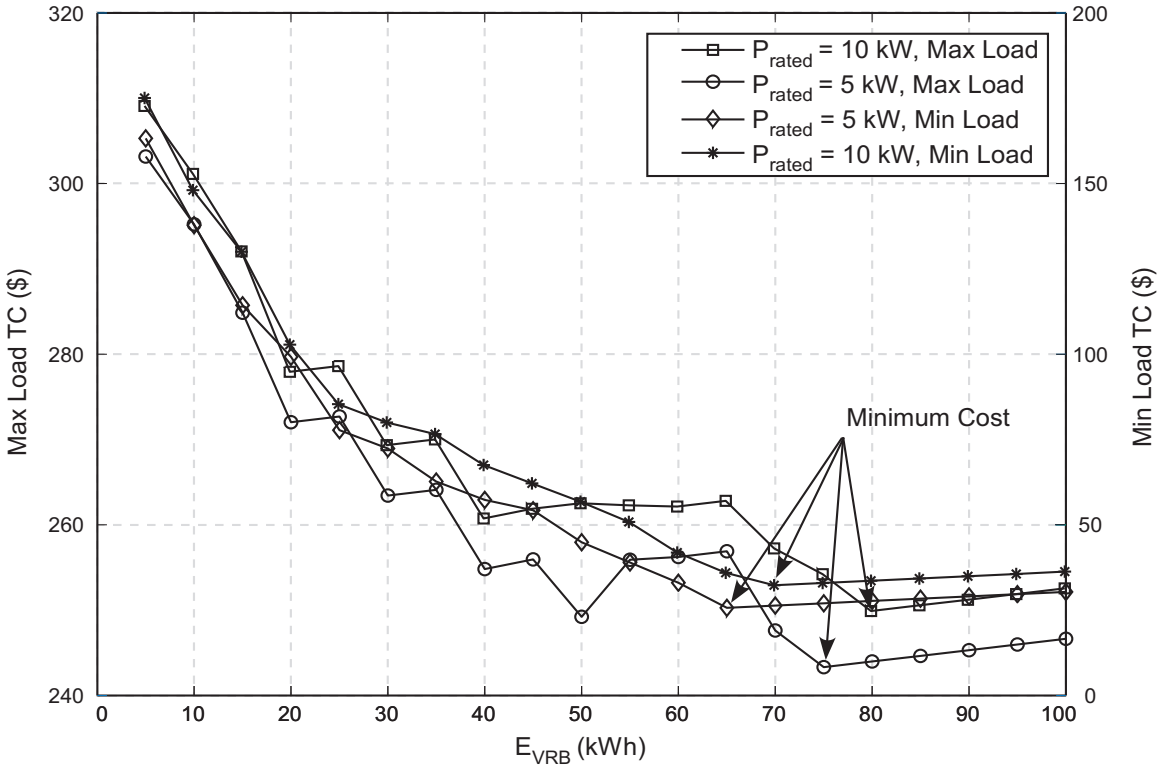

Fig. 9: Costs for operation in September 2013 at minimum and maximum load for a power rating P_{vrb}^{rated} of 5 kW and 10 kW

the load at 16:00 hours to keep the diesel generator off during light load. Also note that the diesel generator is off for the majority of the sunlight hours during which the solar array can simultaneously serve the load and charge the VRB according to Constraint R5. According to Constraint R3, the VRB is always charged or discharged when its efficiency is high (see Fig. 2).

This process is repeated for the remaining three operating profiles of December 2012, March 2013, and September 2013. For example, similar results for September 2013 are shown in Figures 9 – 11. In this month, the optimum energy rating shows more variation than in June, but there is still consistency.

The minimum cost and energy rating across all months and power ratings for minimum loading is given in Table III. Similarly, the minimum cost and energy rating

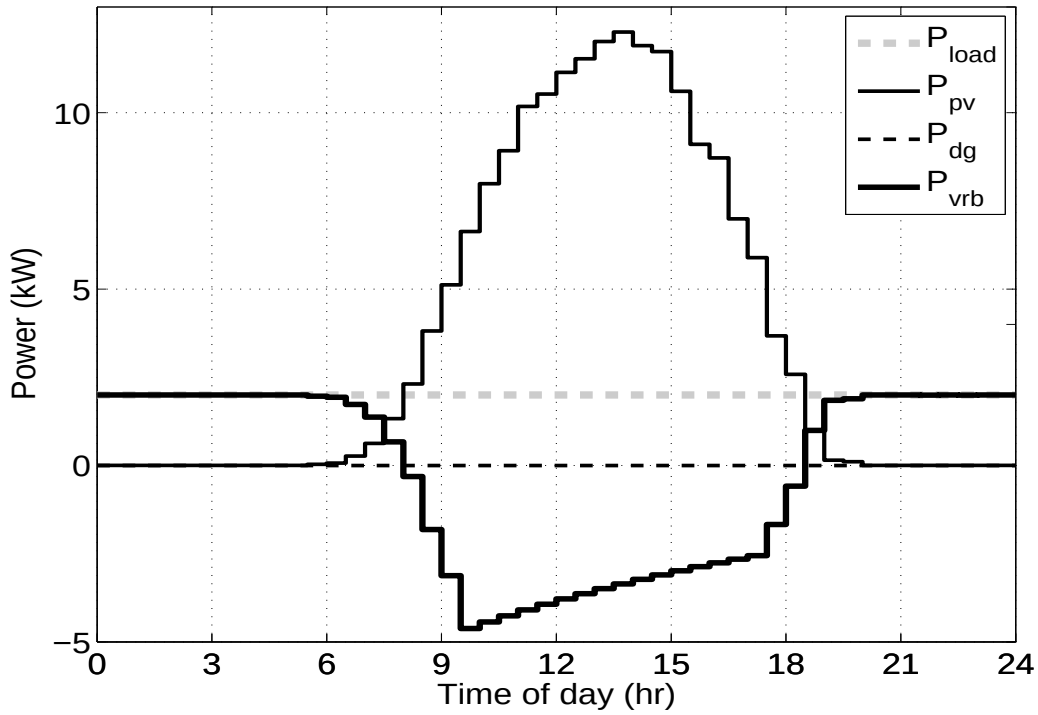

Fig. 10: Dispatch on one day of September 2013 at minimum load and $P_{VRB}^{rated} = 5$ kW and $E_{VRB}^{rated} = 65$ kWh

across all months and power ratings for maximum loading is given in Table IV.

TABLE III: Optimum Cost and Energy Rating at Minimum Load

P_{vrb}^{rated} (kW)	Dec 12 ($, kWh)	Mar 13 ($, kWh)	Jun 13 ($, kWh)	Sep 13 ($, kWh)
5	(277, 5)	(128, 30)	(25, 60)	(27, 65)
10	(283, 5)	(134, 30)	(32, 65)	(32, 70)

From these results, it is possible to select the rating of the VRB based on the optimum costs. As expected, the lowest costs occur during the months in which there is the largest amount of solar insolation. Note that the PV arrays are rated at 15 kW. The PV panels seldom output their maximum rated power and only do so for a short

TABLE IV: Optimum Cost and Energy Rating at Maximum Load

P_{vrb}^{rated} (kW)	Dec 12 ($, kWh)	Mar 13 ($, kWh)	Jun 13 ($, kWh)	Sep 13 ($, kWh)
5	(475, 5)	(347, 5)	(247, 65)	(243, 75)
10	(480, 5)	(359, 5)	(257, 65)	(250, 80)

period of time during the day (for fixed mounting panels) and for a few months of the year. Thus only for a limited time is there any potential advantage for the extra power capacity provided by the 10 kW VRB and as the optimum costs indicate, the 10kW VRB is never cost effective. In evaluating the energy ratings of the VRB, the optimal size can be selected by noting the optimal rating sizes for the seasons in which energy storage is effective. For both minimum and maximum loading profiles, a VRB rated (5 kW, 65 kWh) provides the best cost performance over the longest period of time.

The disclaimer to these conclusions is that the VRB power and energy ratings must be evaluated based on the typical insolation profile and diesel fuel cost for the location in which the system is to be located, but the evaluation procedure will remain the same.

B. Case Study II - Grid-connected Microgrid

Based on the operating strategies of a grid-connected microgrid, the utility grid can be treated as a back-up or the main source of power. The former operating strategy is often used when the accessibility to the grid is limited while the latter one is applied when the fuel supplies for the diesel generators are limited.

TABLE V: Optimum Cost and Energy Rating at Minimum Load

P_{vrb}^{rated} (kW)	Dec 12 ($, kWh)	Mar 13 ($, kWh)	Jun 13 ($, kWh)	Sep 13 ($, kWh)
5	(277, 5)	(120, 30)	(23, 60)	(22, 65)
10	(283, 5)	(131, 30)	(31, 65)	(29, 70)

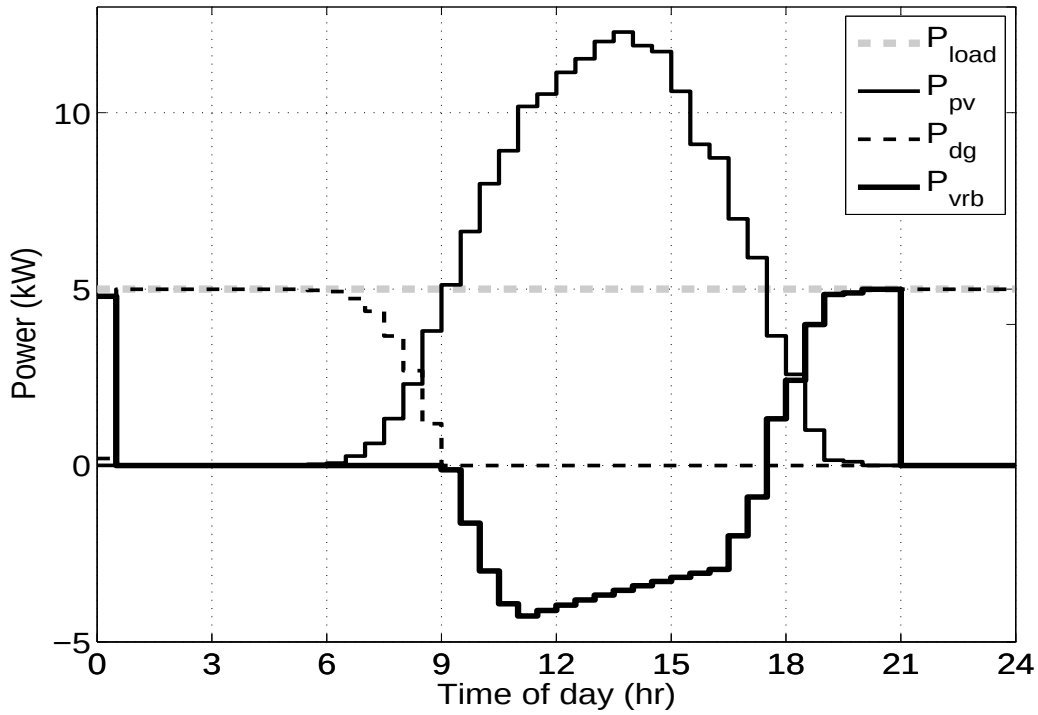

Fig. 11: Dispatch on one day of September 2013 at maximum load and $P_{VRB}^{rated} = 5$ kW and $E_{VRB}^{rated} = 65$ kWh

1) Case II.1: In this case, the microgrid's diesel generators are the main sources to balance the system's load. The grid power is only used to cover the peak load in a short period of time. As shown in Table V and Table VI, the results are slightly different from those of the isolated system from Case study I. It is because of the fact that the exchanged power between the microgrid and the grid is too small to have significant

TABLE VI: Optimum Cost and Energy Rating at Maximum Load

P_{vrb}^{rated} (kW)	Dec 12 ($, kWh)	Mar 13 ($, kWh)	Jun 13 ($, kWh)	Sep 13 ($, kWh)
5	(475, 5)	(339, 5)	(242, 65)	(238, 75)
10	(480, 5)	(357, 5)	(256, 65)	(249, 80)

impact on the total cost per day. Therefore, the optimal VRB's ratings are similarly chosen at $(5KW, 65kWh)$.

2) Case II.2: In this case, the microgrid's diesel generators are only used as back-up source of power. The system's load is mainly powered by the grid or the PV arrays. Results are shown in Table VII and Table VIII. The optimal total costs per day for different months of the year are observed at the minimum power and energy ratings of the VRB - $5kW/5kWh$ in most scenarios. The VRB is only cost effective serving minimum load in September when the PV power is high. This is because the investment cost of the VRB is high compared to the electricity cost of the utility grid, therefore the VRB is not cost effective in most scenarios when a grid-tie is available.

TABLE VII: Optimum Cost and Energy Rating at Minimum Load

P_{vrb}^{rated} (kW)	Dec 12 ($, kWh)	Mar 13 ($, kWh)	Jun 13 ($, kWh)	Sep 13 ($, kWh)
5	(33, 5)	(24, 5)	(17, 20)	(15, 25)
10	(39, 5)	(31, 5)	(24, 5)	(22, 20)

TABLE VIII: Optimum Cost and Energy Rating at Maximum Load

P_{vrb}^{rated} (kW)	Dec 12 ($, kWh)	Mar 13 ($, kWh)	Jun 13 ($, kWh)	Sep 13 ($, kWh)
5	(62, 5)	(49, 5)	(41, 5)	(39, 5)
10	(68, 5)	(55, 5)	(47, 5)	(46, 5)

VI. CONCLUSIONS

In this paper, an analytical approach has been developed for optimal sizing of VRB storage system for isolated microgrids. Non-linear charge/discharge efficiencies and operating characteristics of VRB system are considered in the system's constraints. The feasibility of the solution is ensured based on per-day cost model. The method can also be valid for optimal sizing different types of ESSs if the cost and efficiency model

are known. Case studies have been performed to find optimal VRB power and energy ratings for both isolated and grid-connected microgrids considering different scenarios of load and insolation. The results show the optimal solution occurs when the operating cost benefit by increasing VRB capacity can justify the increment in investment capital.

References

[1] S. Bahramirad, W. Reder, and A. Khodaei, "Reliability-constrained optimal sizing of energy storage system in a microgrid," *Smart Grid, IEEE Transactions on*, vol. 3, no. 4, pp. 2056–2062, 2012.

[2] B. Borowy and Z. Salameh, "Methodology for optimally sizing the combination of a battery bank and pv array in a wind/pv hybrid system," *Energy Conversion, IEEE Transactions on*, vol. 11, no. 2, pp. 367–375, 1996.

[3] M. Elhadidy and S. Shaahid, "Optimal sizing of battery storage for hybrid (wind+diesel) power systems," *Renewable Energy*, vol. 18, no. 1, pp. 77 – 86, 1999.

[4] P. Arun, R. Banerjee, and S. Bandyopadhyay, "Optimum sizing of battery-integrated diesel generator for remote electrification through design-space approach," *Energy*, vol. 33, no. 7, pp. 1155 – 1168, 2008.

[5] M. R. Aghamohammadi and H. Abdolahinia, "A new approach for optimal sizing of battery energy storage system for primary frequency control of islanded microgrid," *International Journal of Electrical Power & Energy Systems*, vol. 54, no. 0, pp. 325 – 333, 2014.

[6] S. Chen, H. Gooi, and M. Q. Wang, "Sizing of energy storage for microgrids," *Smart Grid, IEEE Transactions on*, vol. 3, no. 1, pp. 142–151, 2012.

[7] H. T. Le and T. Q. Nguyen, "Sizing energy storage systems for wind power firming: An analytical approach and a cost-benefit analysis," in *Power and Energy Society General Meeting - Conversion and Delivery of Electrical Energy in the 21st Century, 2008 IEEE*, 2008, pp. 1–8.

[8] M. Ross, R. Hidalgo, C. Abbey, and G. Joos, "Analysis of energy storage sizing and technologies," in *Electric Power and Energy Conference (EPEC), 2010 IEEE*, 2010, pp. 1–6.

[9] T. Nguyen, X. Qiu, J. D. Guggenberger, M. L. Crow, and A. C. Elmore, "Performance characterization for photovoltaic-vanadium redox battery microgrid systems," *IEEE Transactions on Sustainable Energy*, 2013, Revised and Resubmitted.

[10] S. M. Schoenung and W. V. Hassenzahl, "Long- vs. short-term energy storage technologies analysis - a life-cycle cost study," Sandia National Laboratories, Albuquerque SAND2003-2783, Tech. Rep., 2003.

[11] EPRI, "Vanadium redox flow batteries, an in-depth analysis," EPRI, Tech. Rep., 2007.

[12] O. Skarstein and K. Ulhen, "Design considerations with respect to long-term diesel saving in wind/diesel plants," *Wind Engineering*, vol. 13(2), pp. 72–87, 1989.

[13] L. Rodolfo Dufo and A. Jose L. Bernal, "Multi-objective design of pv-wind-diesel-hydrogen-battery systems," *Renewable Energy*, vol. 33, no. 12, pp. 2559 – 2572, 2008.

[14] T. Nguyen and M. Crow, "Optimization in energy and power management for renewable-diesel microgrids using dynamic programming algorithm," in *Cyber Technology in Automation, Control, and Intelligent Systems, 2012 IEEE International Conference on*, 2012, pp. 11–16.

[15] Strategic Environmental Research and Development Program (SERDP), "Sustainable Forward Operating Bases," August 2010.

[16] "Rural Fuel Pricing in Alaska," [Online]. Available: http://www.law.state.ak.us/pdf/civil/ 021810RuralFuelPricinginAlaska.pdf.

[17] "Electric Power Monthly,",2014, [Online]. Available: http://www.eia.gov/electricity/monthly/pdf/epm.pdf.

III. STOCHASTIC OPTIMIZATION OF RENEWABLE-BASED MICROGRID OPERATION INCORPORATING BATTERY OPERATION COST

Tu A. Nguyen, M. L. Crow, *IEEE Fellow*

Department of Electrical and Computer Engineering

Missouri University of Science and Technology, Rolla, MO 65401

Abstract

Integration of renewable energy resources in microgrids has been increasing in the recent decades in response to the concerns of climate change and rising fuel prices. Due to the randomness in the renewable resources such as solar and wind, the actual renewable power generation can deviate from the forecast values incurring extra operation cost for committing costly reserve units or penalty cost for shedding the loads. In addition, it is often desired to charge/discharge and coordinate the energy storage units in an efficient and economical way. To address these problems, a novel battery operation cost model is proposed in this paper which allows to consider a battery as an equivalent fuel-run generator. A probabilistic constrained approach is used to incorporate the uncertainties of renewable sources and load demands into the unit commitment (UC) and economic dispatch (ED) problems. The UC is solved using stochastic dynamic programming. The result of stochastic UC is presented in comparison with the deterministic UC in a case study of a typical microgrid.

Index Terms

Microgrids, renewable energy, energy storage, vanadium redox battery, optimal scheduling, unit commitment, economic dispatch

I. INTRODUCTION

During the past decades, the electric power industry has been reshaping in response to the rising concerns about global climate change and fast increasing fossil fuel prices. For a more efficient, reliable and environmentally friendly energy production, it is critical to increase the deployment of distributed generation (DG), especially from renewable energy resources (RE), as well as distributed energy storage (DS). This trend has brought forth the concept of ”Microgrid” which can be understood as a cluster of distributed energy resources, energy storage and local loads, managed by an intelligent energy management system (EMS)[1]. The advantages of microgrids over the traditional distribution systems exhibit in many aspects: energy losses reduction due to the proximity between DGs and loads, reliability improvement with the ability to work in islanded mode during system faults, transmission and distribution lines relief via efficient energy management to reduce energy import from the grid[2].

As similar to the main grid operation, microgrid operation can be determined by unit commitment (UC) and economy dispatch (ED). The UC is performed from one day to one week ahead providing the start-up and shut-down schedule for each generation and storage unit which can minimize the operation cost of the microgrid. After UC is taken place, ED is performed from few minutes to one hour in advance to economically allocate the demand to the running units considering all unit and system constraints[3].

Although the optimization of operation for the conventional power systems have been well studied in the literature, the proposed methods cannot be applied directly to microgrids with high integration of RE and ES devices. Specifically, due to the stochastic nature of the renewable resources such as solar and wind, the actual renewable power generation can be far different from the forecast values incurring extra operation cost for committing costly reserve units or penalty cost for curtailing the demands. In addition, to better utilize the renewable energy in the microgrid it is necessary to charge/discharge and coordinate the energy storage units in an efficient and economical way. To address these problems, the stochastic model of renewable energy and load demands as well as

the working characteristics and operational cost of the ES devices should be incorporated into the UC and ED problems.

In the specialized literature, studies related to stochastic optimization for renewable-based microgrids operation have been conducted. In [4], microgrid day-ahead scheduling is addressed as a two-stage stochastic problem in which the first stage identifies the optimal dispatch for the distributed units while the second stage considers the variability and uncertainty of photovoltaic (PV) and wind energy generation. The outputs of PV and wind generation units are considered in different scenarios generated by Monte Carlo simulation. The optimization of unit commitment, which is a mixed non-linear programming problem, is solved by iteration method using CPLEX. The probabilistic UC in [5] is similarly formulated as a two-stage stochastic programming problem in order to incorperate the uncertainty in load and PV forecast. Forecast errors are modelled by normal distribution. Two-stage stochastic programming is also used in [6],[7].

Scenario-based stochastic programming for microgrid operation is proposed in [8],[9],[10]. The scenarios of PV, wind generations and load demands are respectively generated by Roulette Wheel Mechanism (RWM), Lattice Monte Carlo Simulations (LMCS) and Latin hypercube sampling (LHS). The repeated and low-probability scenarios are then removed in [8],[9] while in [10] K-means clustering algorithm is used to reduce the number of scenarios. The stochastic optimization of UC is solved by Adaptive Modified Firefly Algorithm in [8] and by TeachingLearning-Based Optimization (TLBO) algorithm in [9].

In [11], the economic dispatch problem optimizes fuel as well as green-house gas emission cost. Expected values and cumulative probability functions (CDF) of PV and wind power outputs based on Beta and Weibull distributions, respectively. The CDF of total required reserve is obtained by the convolution CDF of PV and wind power. The multi-objective optimization is solved using genetic algorithm. The ED in [12] is similarly addressed and solved by Particle Swarm Optimization (PSO). In [13], microgrid ED is formulated by wait-and-see approach. Cost optimization of the stochastic ED is

solved by an improved PSO; means and standard deviations of optimal solutions are are determined by two-point estimate method. In [14], a discrete probabilistic model is proposed considering the intermittency of renewable power sources through the estimation of the probability density function (PDF) of the generator output powers. A model for ED and demand-side management is developed for in a power system with multiple wind farms in [15]. The loss of load probability (LOLP) is considered as a constraint in ED to improve the reliability of the system.

As observed in the literature, the majority of existing studies is based on Scenario-based stochastic programming [4]-[9]. This approach is based on replication of deterministic models across scenarios which generated by MCS in most of the works. The computational burden in this approach increases exponentially to the number of investigated scenarios thereby increasing significantly computational cost [2]. Scenario reduction using different techniques, as seen in the previous studies, might ease the problem; however, it can neglect the low-probability but high-impact scenarios. Therefore, we propose a probabilistic constrained approach to incorporate the uncertainties into the UC and ED for microgrids. In this approach, the perfect holding of power balance is relaxed by introducing a probabilistic constraint which contains renewable powers and load demands as random variables. The constraint is enforced with high probability while the penalty for constraint violation is applied in the cost function. The advantage of this method over the scenario based method is that all possibilities of load demands and renewable generations are covered without considering a large number of scenarios. In this paper, stochastic dynamic programming is used to solve the UC.

Regarding to energy storage management in microgrids, most of the previous studies [4]-[15] assumed the energy storage as a single battery with constant efficiency and zero operational cost. For this assumption, the ED tends to dispatch as much power as possible to charge/discharge the battery regardless of its performance and state of health (SOH). In practice, multiple ES technologies, which are different in terms of cycling life time, efficiencies and working characteristics, may co-exist in a microgrid. Therefore,

it is necessary to optimally dispatch power to multiple storage units considering their life time, efficiencies and working characteristics. In [16][17], efficiencies of different storage technologies are characterized as functions of charge/discharge power. In [16], an objective is defined to optimize the total charge/discharge efficiencies of ES devices; however, the problem is simplified by priority list method. In this paper, we propose a novel battery operation cost model which allows to consider a battery as an equivalent fossil fuel generator in the UC and ED. The model accounts for charge/discharge efficiencies, life time and capacity degradation of the batteries.

Specifically, the following contributions are made in this paper:

- A novel battery operation cost model is propose accounting for charge/discharge efficiencies as well as cycling life time of the batteries. The model allows to treat a battery as an equivalent fossil fuel generator in the UC and ED.
- A probabilistic constrained approach is proposed to incorporate the uncertainties of renewable sources and load demands in microgrids into the UC and ED problems. The UC is solved using stochastic dynamic programming.

II. BATTERY OPERATION COST MODEL

For a small-scale fossil fuel generator in microgrids, the operation cost is typically the fuel cost which is fuel price times fuel consumption. The cost can be characterized as a function of its output power as following [3, 10]:

$$\begin{aligned} F_{gen}(P_{gen}) &= c_{gen}.H_{gen}(P_{gen})(\$/h) \\ &= c_{gen}[a_g P_{gen}^2 + b_g P_{gen} + c_g](\$/h) \end{aligned} \tag{1}$$

where $c_{gen}(\$/gal)$ is fuel price, $H_{gen}(P_{gen})(gal/h)$ is fuel consumption and $P_{gen}(kW)$ is output power of generator i.

Different from a generator, a battery such as lead-acid or lithium-ion consumes no fuel to run. This is a challenge to evaluate the operation cost of a battery. However,

in terms of energy conversion process, a battery and a generator are analogous. In a generator, energy is stored in fuel form and generated in electricity form via combustion process. Similarly, in a battery, electricity is charged and discharged via electrochemical process. In general, charging a battery is analogous to refilling fuel for a generator; thus, the input electricity (kWh) can be considered as the "fuel" for the battery. We call it kWh_f to emphasize the analogy. Therefore, the operation cost of a battery can be determined in the same form as (1) by deriving kWh_f price and kWh_f consumption of the battery. In this paper, lead-acid, lithium-ion and vanadium redox battery are investigated.

A. kWh_f Price for Battery

For a generator, the price of fossil fuel $c_{gen}(\$/gal)$ is composed of two components as follow:

$$c_{gen} = c_{gen}^{fuel} + c_{gen}^{avai}(\$/gal) \tag{2}$$

in which c_{gen}^{fuel} represents the cost for fuel and c_{gen}^{avai} represents availability cost . The availability cost includes fuel transportation cost and other service costs such as cost for on-site storage facility. Depending on the location of the generator, c_{gen} can be much larger than c_{gen}^{fuel} due to transportation and other service cost. For example, delivering fuel to rural areas of Alaska is complicated and expensive, since fuel must typically be delivered by either barge or plane [18].

Similarly, kWh_f price for a battery can be determined as:

$$c_{bat} = c_{bat}^{kWh_f} + c_{bat}^{avai}(\$/kWh_f) \tag{3}$$

where $c_{bat}^{kWh_f}$ is the price of energy used to charge the battery and c_{bat}^{avai} represents the availability cost of battery capacity. In a microgrid, if renewable energy is used to charge the battery, $c_{bat}^{kWh_f}$ can be zero; therefore, c_{bat}^{avai} is the main portion of the price. c_{bat}^{avai} can be defined as the cost to have $1kWh$ storage capacity available:

$$c_{bat}^{avai} = \frac{ReplacementCost}{C_{\Sigma}}(\$/kWh_f) \tag{4}$$

where C_{Σ} is the total lifetime cycling capacity of a battery. By convention, an electrochemical battery such as lead acid and lithium-ion is often considered to be at the end of its life (EOL) when it has degraded to 80% of its rated energy capacity [19]. Assuming that a battery will be discharged to its rated depth of discharge (DOD) every cycle, the average capacity degradation rate is $\frac{0.2}{L_r}C_r(kWh/cycle)$ in which $C_r(kWh)$ is the battery rated capacity and $L_r(cycle)$ is the rated life time.

Different from a lead acid or a lithium-ion battery, a vanadium redox battery (VRB) has no capacity degradation from repeated deep discharge and recharge. Cycle life of a VRB mainly depends on the life expectancy of its Proton Exchange Membrane (PEM) and its pumps. A VRB can last over 10000 cycles until its membrane degradation or pumps failure.

Therefore, total lifetime usable capacity of a battery can be estimated as follow:

- Lead acid and lithium-ion battery:

$$C_{\Sigma} = C_r DOD_r[L_r - \frac{0.2}{L_r}(1 + 2 + ... + L_r)](kWh) \tag{5}$$

$$= C_r DOD_r(0.9L_r - 0.1)(kWh) \tag{6}$$

- Vanadium redox battery:

$$C_{\Sigma} = C_r DOD_r L_r(kWh) \tag{7}$$

B. kWh_f Consumption for Battery

kWh_f consumption of a battery during discharge is defined as the energy usage (kWh_f) for supplying a load during a unit time:

$$H_{bat} = P_{bat}^{\Sigma} = P_{bat}^{d} + P_{bat}^{ld}(kWh_f/h) \tag{8}$$

in which $P_{bat}^{d}(kW)$ is the battery output power, $P_{bat}^{ld}(kW)$ is the power loss during discharge.

kWh_f consumption of a battery during charge is defined as the energy loss (kWh_f) for charging the battery during a unit time:

$$L_{bat} = P_{bat}^{lc}(kWh_f/h) \tag{9}$$

in which $P_{bat}^{c}(kW)$ is the battery charge power, $P_{bat}^{lc}(kW)$ is the power loss during charge.

Depending on battery type, H_{bat} and L_{bat} can be characterized as functions of P_{bat}^{d} and P_{bat}^{c}, respectively. In this section, H_{bat} and L_{bat} are characterized for lead-acid, lithium-ion and vanadium redox battery.

1) Lead acid and lithium-ion battery: The power loss of lead-acid and li-ion battery is mainly caused by the heat loss during charge or discharge. The heat is generated by ohmic resistances of the electrodes and electrolytes, and also by polarization effects [20]. The power loss is proportional to the voltage drop (polarization)caused by the current:

$$P_{joule} = \Delta V \times I(kW) \tag{10}$$

For lead-acid and lithium-ion battery, the voltage drop can be determined based on the empirical method proposed in [21]:

- During discharge:

$$\Delta V = (R + \frac{K}{SOC})I + \frac{Q_r.K(1 - SOC)}{SOC} \tag{11}$$

- During charge:

$$\Delta V = (R + \frac{K}{0.9 - SOC})I + \frac{Q_r.K(1 - SOC)}{SOC} \tag{12}$$

where $R(\Omega)$ is the internal ohmic resistance, K is a constant which can be calculated from manufacturer's data, $Q_r(Ah)$ is the rated capacity of the battery.

From (11),(12), kWh_f consumption during charge and discharge for lead acid and lithium-ion battery can be determined as follow:

- During discharge:

$$\begin{aligned} P_{bat}^{ld} &= 10^{-3}[(R+\frac{K}{SOC})I^2+\frac{Q_r.K(1-SOC)}{SOC}I] \\ &\approx \frac{10^3(R+\frac{K}{SOC})}{V_r^2}(P_{bat}^d)^2+\frac{10^3C_r.K(1-SOC)}{SOC.V_r^2}P_{bat}^d \\ H_{bat} &= P_{bat}^d+P_{bat}^{ld}(kWh_f/h) \end{aligned} \tag{13}$$

- During charge:

$$\begin{aligned} P_{bat}^{lc} &= (R+\frac{K}{1.1-SOC})I^2+\frac{Q_r.K(1-SOC)}{SOC}I \\ &\approx \frac{10^3(R+\frac{K}{1.1-SOC})}{V_r^2}(P_{bat}^c)^2+\frac{10^3C_r.K(1-SOC)}{SOC.V_r^2}P_{bat}^c \\ L_{bat} &= P_{bat}^{lc}(kWh_f/h) \end{aligned} \tag{14}$$

with SOC is the state of charge, V_r is the rated voltage of battery.

2) Vanadium redox battery: The power loss of a vanadium redox battery during charge and discharge includes two components: power for pumping the electrolytes and stack loss power due to internal resistance and electrochemical process. Based on the empirical proposed in [17], open circuit voltage, stack voltage can be characterized as functions of SOC and charge/discharge power:

- Open circuit voltage:

$$V_{oc} = a_v^o SOC + b_v^o(V) \tag{15}$$

- During discharge:

$$I_{stack}^d = a_i^d P_{bat}^d + b_i^d SOC + c_i^d(A) \tag{16}$$

- During charge:

$$I^c_{stack} = (a^c_i SOC + b^c_i)P^c_{bat} + c^c_i SOC + d^c_i(A) \tag{17}$$

All model coefficients are given in Table I where $V_r(V)$ and $I_r(A)$ are the rated voltage and rated current of the VRB.

TABLE I: VRB loss model coefficients

(i,k)	a^i_k	b^i_k	c^i_k	d^i_k
(o,v)	$0.2414V_r$	$0.9925V_r$	$-$	$-$
(d,i)	$\frac{1.0719}{V_r \times 10^{-3}}$	$0.0183I_r$	$0.0210I_r$	$-$
(c,i)	$\frac{-0.3093}{V_r \times 10^{-3}}$	$\frac{1.0397}{V_r \times 10^{-3}}$	$0.0604I_r$	$-0.122I_r$

From (16),(17), kWh_f consumption during charge and discharge for VRB can be determined as follow:

- During discharge:

$$\begin{aligned} H_{bat} &= 10^{-3} I^d_{stack} V_{oc}(kWh_f/h) \\ &= 10^{-3}(a^o_v SOC + b^o_v)[a^d_i P^d_{bat} + (b^d_i SOC + c^d_i)] \end{aligned} \tag{18}$$

- During charge:

$$\begin{aligned} L_{bat} &= P^c_{bat} - 10^{-3} I^c_{stack} V_{oc}(kWh_f/h) \\ &= [1 - 10^{-3}(a^o_v SOC + b^o_v)(a^c_i SOC + b^c_i)]P^c_{bat} \\ &\quad - 10^{-3}(a^o_v SOC + b^o_v)(c^c_i SOC + d^c_i) \end{aligned} \tag{19}$$

III. STOCHASTIC UNIT COMMITMENT FOR MICROGRIDS

A. Problem Formulation

In this paper, the stochastic unit commitment is formulated to minimize the expected operation cost of a microgrid over a time horizon N. The objective function is as follow:

$$minC = \sum_{k=1}^{N}(F_k + S_k) \tag{20}$$

$$F_k = \mathbb{E}\left\{F_{g,k} + F^d_{b,k} + F^c_{b,k} + F_{m,k}\right\} \tag{21}$$

in which,

$$F_{g,k} = \sum_{i=1}^{n_1} s_{gi,k} F_{gi}(P_{gi,k})T = \sum_{i=1}^{n_1} s_{gi,k} c_{gi} H_{gi}(P_{gi,k})T \tag{22}$$

$$F^d_{b,k} = \sum_{i=1}^{n_2} s^d_{bi,k} F^d_{bi}(P^d_{bi,k})T = \sum_{i=1}^{n_2} s^d_{bi,k} c_{bi} H^d_{bi}(P^d_{bi,k})T \tag{23}$$

$$F^c_{b,k} = \sum_{i=1}^{n_2} s^c_{bi,k} F^c_{bi}(P^c_{bi,k})T = \sum_{i=1}^{n_2} s^c_{bi,k} c_{bi} L^c_{bi}(P^c_{bi,k})T \tag{24}$$

$$F_{m,k} = F_m(P_{m,k})T \tag{25}$$

$$\tag{26}$$

where

- N is the time horizon, $T(hr)$ is the time step;
- F_k is the total expected operation cost in period k; S_k is the total transition cost which accounts for the start-up and shut-down cost of the generators in period k .
- $n1$ and $n2$ are the number of generators and batteries, respectively;
- gi and bi denote generator i and battery i, respectively;
- $F_{g,k}, F^d_{b,k}, F^c_{b,k}(\$)$ are respectively the total operation cost during period k of the generators, the discharging batteries and the charging batteries; $F_{m,k}$ is the cost due to power mismatch;
- $s_{gi,k}, s^d_{bi,k}, s^c_{bi,k}$ are respectively the binary status during period k of the generator i

and battery i; $AND(s^d_{bi,k}, s^c_{bi,k}) = 0$ due to the fact that a battery could not charge and discharge at the same time.

- $c_{gi}(\$/gal)$ is the fuel price for generator i; $c_{bi}(\$/kWh_f)$ is the kWh_f price for battery i;
- $H_{gi}(gal/h)$ is the fuel consumption of generator i; $H_{bi}(kWh_f/h)$ and $L_{bi}(kWh_f/h)$ are respectively the kWh_f consumptions during discharging and charging of battery i;
- $P_{gi,k}, P^d_{bi,k}, P^c_{bi,k}(kW)$ are respectively the dispatched power during period k to generator i, discharging battery i and charging battery i; $P_{m,k}$ is the power mismatch during period k.

To better define the problem, the following conventions are introduced:

- Charging power $P^c_{bi,k}$ is considered as negative generation.
- Renewable sources (PV and Wind turbines generators) are not dispatchable and considered as a negative load. The net load at period k is defined as:

$$P_{net,k} = \sum P_{load,k} - \sum P_{PV,k} - \sum P_{W,k}$$

Since $P_{load,k}, P_{PV,k}, P_{W,k}$ are random, $P_{net,k}$ is considered as a random variable.

- The batteries are charged only when $P_{net,k} < 0$.
- The power mismatch $P_{m,k}$ during period k is the difference between total generation and the net load defined as follow:
  - If $P_{net,k} \geq 0$

$$\begin{aligned} P_{m,k} &= P_{gen,k} - P_{net} \\ P_{gen,k} &= \sum_{i=1}^{n_1} s_{gi,k} P_{gi,k} + \sum_{i=1}^{n_2} s^d_{bi,k} P^d_{bi,k} \end{aligned} \tag{27}$$

with $P_{gen,k} > 0$ is the total generation.

– If $P_{net,k} < 0$

$$P_{m,k} = P_{chg,k} - P_{net}$$
$$P_{chg,k} = \sum_{i=1}^{n_2} s^c_{bi,k} P^c_{bi,k} \tag{28}$$

with $P_{chg,k} < 0$ is the total charge.

- The microgrid is grid connected. The electricity price and buy back price are considered as deterministic.

The constraints of the problem are defined based on the energy management strategies and physical limits of the devices in the microgrid. The following constraints are considered:

- $R1$- The power mismatch is greater than zero with a predefined probability.
- $R2$- One battery should not be discharged to charge another battery; Generators should not be used to charge the batteries.
- $R3$- Each storage device cannot be charged (or discharged) beyond the maximum (or minimum) SOC.
- $R4$- The charge (or discharge) rate for each storage device should not exceed the maximum (or minimum) rates.
- $R5$- Each generator should not be low loading when online.
- $R6$- Once a generator is brought online, it should remain online for a minimum set time; when a generator is powered off, it should remain off a minimum time before it can be restarted.

The above constraints are formulated as follow:

$$R1: \begin{cases} \mathbb{P}(P_{m,k} \geq 0 \cap P_{net,k} > 0) = \alpha_k \mathbb{P}(P_{net,k} > 0) \\ \mathbb{P}(P_{m,k} \geq 0 \cap P_{net,k} < 0) = \beta_k \mathbb{P}(P_{net,k} < 0) \\ \text{with } \alpha_k, \beta_k \in [0,1] \end{cases}$$

$$R2: \begin{cases} AND(s^d_{bi,k}, s^c_{bj,k}) = 0 \quad \forall i,j \\ AND(s_{gi,k}, s^c_{bj,k}) = 0) \quad \forall i,j \end{cases}$$

$$R3: SOC_{bi}^{min} \leq SOC_{bi,k} \leq SOC_{bi}^{max}$$

$$R4: \begin{cases} P_{bi}^{min,d} \leq P_{bi,k}^{d} \leq P_{bi}^{max,d} & \text{if } bi \text{ is discharging} \\ P_{bi}^{min,c} \leq P_{bi,k}^{c} \leq P_{bi}^{max,c} & \text{if } bi \text{ is charging} \end{cases}$$

$$R5: P_{gi}^{min} \leq P_{gi,k} \leq P_{gi}^{max}$$

$$R6: \begin{cases} T_{gi,k}^{up} \geq T_{gi}^{up,min} & \text{if } gi \text{ is online} \\ T_{gi,k}^{dw} \geq T_{gi}^{dw,min} & \text{if } gi \text{ is offline} \end{cases}$$

where $SOC_{bi,k}$ is the state of charge of battery i in period k can be updated as follow:

$$SOC_{bi,k} = \begin{cases} SOC_{bi,k-1} - \frac{H(P_{bi,k}^{d})T}{C_{bi}^{r}} & \text{if discharging} \\ SOC_{bi,k-1} + \frac{[P_{bi,k}^{c} - L(P_{bi,k}^{c})]T}{C_{bi}^{r}} & \text{if charging} \end{cases} \tag{29}$$

By enforcing constraint $R1$, $P_{m,k} \geq 0$ will happen in $100\alpha_k\%$ of the time when $P_{net,k} > 0$ and $100\beta_k\%$ of the time when $P_{net,k} < 0$. From (27) and (28), $R1$ can be rewritten as:

$$R1: \begin{cases} \mathbb{P}(0 < P_{net,k} < P_{gen,k}) = \alpha_k \mathbb{P}(P_{net,k} > 0) \\ \mathbb{P}(P_{net,k} < P_{charge,k}) = \beta_k \mathbb{P}(P_{net,k} < 0) \\ \text{with } \alpha_k, \beta_k \in [0,1];\ P_{gen,k} > 0 \text{ and } P_{chg,k} < 0 \end{cases} \tag{30}$$

B. Uncertainties in forecasting error of load demands and renewable sources

To realize the cost function (21) and constraint $R1$, the cumulative distribution function (CDF) and mean value of $P_{net,k}$ need to be specified. In practice, the predicted values of load, PV and wind generation at time period k can be obtained beforehand based on forecast. Therefore, the realization of actual load, PV, wind generation and net load can be expressed as [5, 8, 9]:

$$P_{load,k} = P_{load,k}^{forecast} + \Delta P_{load,k} \tag{31}$$

$$P_{PV,k} = P_{PV,k}^{forecast} + \Delta P_{PV,k} \tag{32}$$

$$P_{WT,k} = P_{WT,k}^{forecast} + \Delta P_{WT,k} \tag{33}$$

$$P_{net,k} = P_{load,k} - P_{PV,k} - P_{WT,k} = P_{net,k}^{forecast} + \Delta P_{net,k} \tag{34}$$

where $\Delta P_{load}, \Delta P_{PV}, \Delta P_{WT}$ are the forecasting errors which mainly depend on the forecasting methods and forecasting horizon. To model the uncertainties of load and renewable source forecast, $\Delta P_{load}, \Delta P_{PV}, \Delta P_{WT}$ are considered as random variables. Although wind power forecast error can be more precisely described with Weibull, Cauchy [22] or mixed Normal-Laplace distribution [23], it can be approximated with a zero mean Normal distribution [24]. Furthermore, the net load error $\Delta P_{net,k}$, which is the sum of all errors, can be approximated with zero mean Normal distribution [24] due to the fact that the load demands and PV generation forecast errors are very close to Normal distribution [5, 8, 9, 24]. The standard deviation of $\Delta P_{net,k}$ can be calculated as follow:

$$\sigma_{net,k} = \sqrt{\sigma^2_{\Delta P_{load}} + \sigma^2_{\Delta P_{PV}} + \sigma^2_{\Delta P_{WT}}} \tag{35}$$

As a result, the following expected values and probabilities can be calculated:

$$1)\ \mathbb{E}(P_{net,k}) = P^{forecast}_{net,k} \tag{36}$$

$$2)\ \mathbb{E}(P_{m,k}|P_{net,k} > 0) = P_{gen,k} - P^{forecast}_{net,k} \tag{37}$$

$$3)\ \mathbb{E}(P_{m,k}|P_{net,k} < 0) = P_{chg,k} - P^{forecast}_{net,k} \tag{38}$$

$$4)\ \mathbb{P}(P_{net,k} < 0) = \Phi\left(-\frac{P^{forecast}_{net,k}}{\sigma_{net,k}}\right) = p_k \tag{39}$$

$$5)\ \mathbb{P}(P_{net,k} > 0) = 1 - p_k \tag{40}$$

$$6)\ \mathbb{P}(0 < P_{net,k} < P_{gen,k}) = \Phi\left(\frac{P_{gen,k} - P^{forecast}_{net,k}}{\sigma_{net,k}}\right) - p_k \tag{41}$$

$$7)\ \mathbb{P}(P_{net,k} < P_{chg,k}) = \Phi\left(\frac{P_{charge,k} - P^{forecast}_{net,k}}{\sigma_{net,k}}\right) \tag{42}$$

where Φ is the CDF of Standard Normal distribution $\mathbb{N}(0, 1)$.

Therefore constraint $R1$ can be realized as:

$$R1: \begin{cases} P_{gen,k} = P_{net,k}^{forecast} + \sigma_{net,k}\Phi^{-1}\left[\alpha_k(1-p_k)+p_k\right] \\ \qquad\qquad\qquad\qquad \text{if } P_{net,k} > 0 \\ P_{chg,k} = P_{net,k}^{forecast} + \sigma_{net,k}\Phi^{-1}\left[\beta_k p_k\right] \\ \qquad\qquad\qquad\qquad \text{if } P_{net,k} < 0 \end{cases}$$

The system will generate (or charge) more or less power by choosing different values of α_k and β_k. Choosing larger α_k will increase the generation while choosing larger β will reduce the charging power. Therefore, depending on energy management policies, α_k and β_k can be flexibly selected. For example, if $\beta_k = 0.5$, 50% chance that the excess power from the renewable energy will be exported to the grid. The expected operation cost in (21) can be expressed as:

$$\begin{aligned} F_k = (1-p_k)(F_{g,k} + F_{b,k}^d + \mathbb{E}\left\{F_{m,k}|P_{net,k}>0\right\}) \\ + p_k(F_{b,k}^c + \mathbb{E}\left\{F_{m,k}|P_{net,k}<0\right\}) \end{aligned} \tag{43}$$

in which

$$\begin{aligned} \mathbb{E}\left\{F_{m,k}|P_{net,k}>0\right\} &= -c_{ex,k}|P_{gen,k} - P_{net,k}^{forecast}|\alpha_k \\ &\quad + c_{im,k}|P_{gen,k} - P_{net,k}^{forecast}|(1-\alpha_k) \end{aligned} \tag{44}$$

$$\begin{aligned} \mathbb{E}\left\{F_{m,k}|P_{net,k}<0\right\} &= -c_{ex,k}|P_{chg,k} - P_{net,k}^{forecast}|\beta_k \\ &\quad + c_{im,k}|P_{chg,k} - P_{net,k}^{forecast}|(1-\beta_k) \end{aligned} \tag{45}$$

with $c_{ex,k}, c_{im,k}$ are the prices of the electricity which are exported to or imported from the grid.

C. Stochastic Dynamic Programming

This UC problem can be categorized as a sequential decision-making problem for which Dynamic Programming (DP) is well known. Dynamic programming (DP) is the method to find the shortest route to the destination by breaking it down to a sequence of

steps overtime; at each step it finds the possible optimum sequences (routes) based on the possible optimum subsequences in the previous steps and finally find the optimum sequence at last step. The main advantage of DP is it can maintain solution feasibility by its ability to find the optimum sub-sequence while searching for the optimum sequence. Dynamic programming can be computationally burdensome. For example, in an N-unit system, there are $2^N - 1$ combinations at each period and for M periods the total number of combinations is $(2^N - 1)^M$[3]. For a large scale system the computation required to traverse this space can be overwhelming. However, in microgrid applications, the small number of units and large number of constraints significantly decrease the search space, therefore dynamic programming can be an appropriate choice of algorithm[17, 25].

Due to the uncertainties associated with the stochastic problem, the cost at each stage is generally a random variable [26]. Therefore, in the stochastic DP technique, the problem is formulated to minimize the expected cost. For applying DP, the states space at stage k is defined as follow:

$$\mathbb{L}_k = \left\{ L_k^1 ... L_k^j ... L_k^{m_k} \right\} \tag{46}$$

$$L_k^j = \left\{ s_{g1,k}^j, ..., s_{gn1,k}^j, s_{b1,k}^{d,j}, ..., s_{bn2,k}^{d,j}, s_{b1,k}^{c,j} ... s_{bn2,k}^{c,j} \right\} \tag{47}$$

where $\mathbb{L}_k$ is the set of feasible states in stage k; m_k is the number of states of $\mathbb{L}_k$; $s_{xi,k}^j$ is the binary status of unit xi which can be a generator, a discharging battery or a charging battery. L_k^j is a valid state if it satisfies constraints $R2$,$R3$, $R6$ and the following conditions:

$$\begin{cases} P_{gen,k}^{min} \leq P_{net,k}^{forecast} + \sigma_{net,k} \Phi^{-1} \left[\alpha_k (1 - p_k) + p_k \right] \leq P_{gen,k}^{max} \\ \qquad\qquad\qquad\qquad\qquad\qquad \text{if } s_{bi,k}^{c,j} = 0 \ \forall i \\ P_{charge,k}^{min} \leq P_{net,k}^{forecast} + \sigma_{net,k} \Phi^{-1} \left[\beta_k p_k \right] \leq P_{charge,k}^{max} \\ \qquad\qquad\qquad\qquad\qquad\qquad \text{otherwise} \end{cases}$$

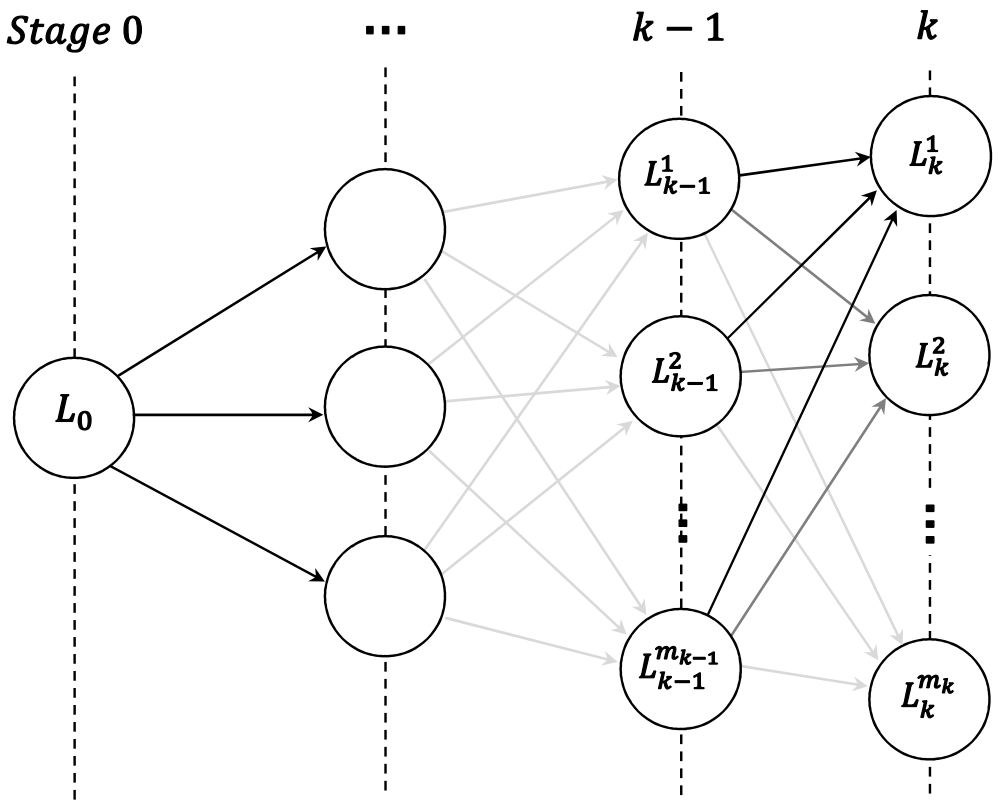

Fig. 1: State space for DP algorithm

In this paper, forward DP algorithm is used (Fig2). The algorithm to compute the minimum cost to arrive state L_k^j in stage k is:

$$C(L_k^j) = \min_{\{\mathbb{L}_{k-1}\}} [F(L_k^j) + S(L_{k-1}^i \to L_k^j) + C(L_{k-1}^i)] \tag{48}$$

where $C(L_k^j)$ is the minimum cost to arrive to state L_k^j; $F(L_k^j)$ is the operating cost for state L_k^j and $S(L_{k-1}^i \to L_k^j)$ is the transition cost from state L_{k-1}^i to state L_k^j.

The operation cost $F(L_k^j)$ can be found by performing ED to minimize the cost function (43) with constraints $R1$, $R4$ and $R5$. In this paper, Steepest Descent algorithm is used to solve the quadratic optimization for ED.

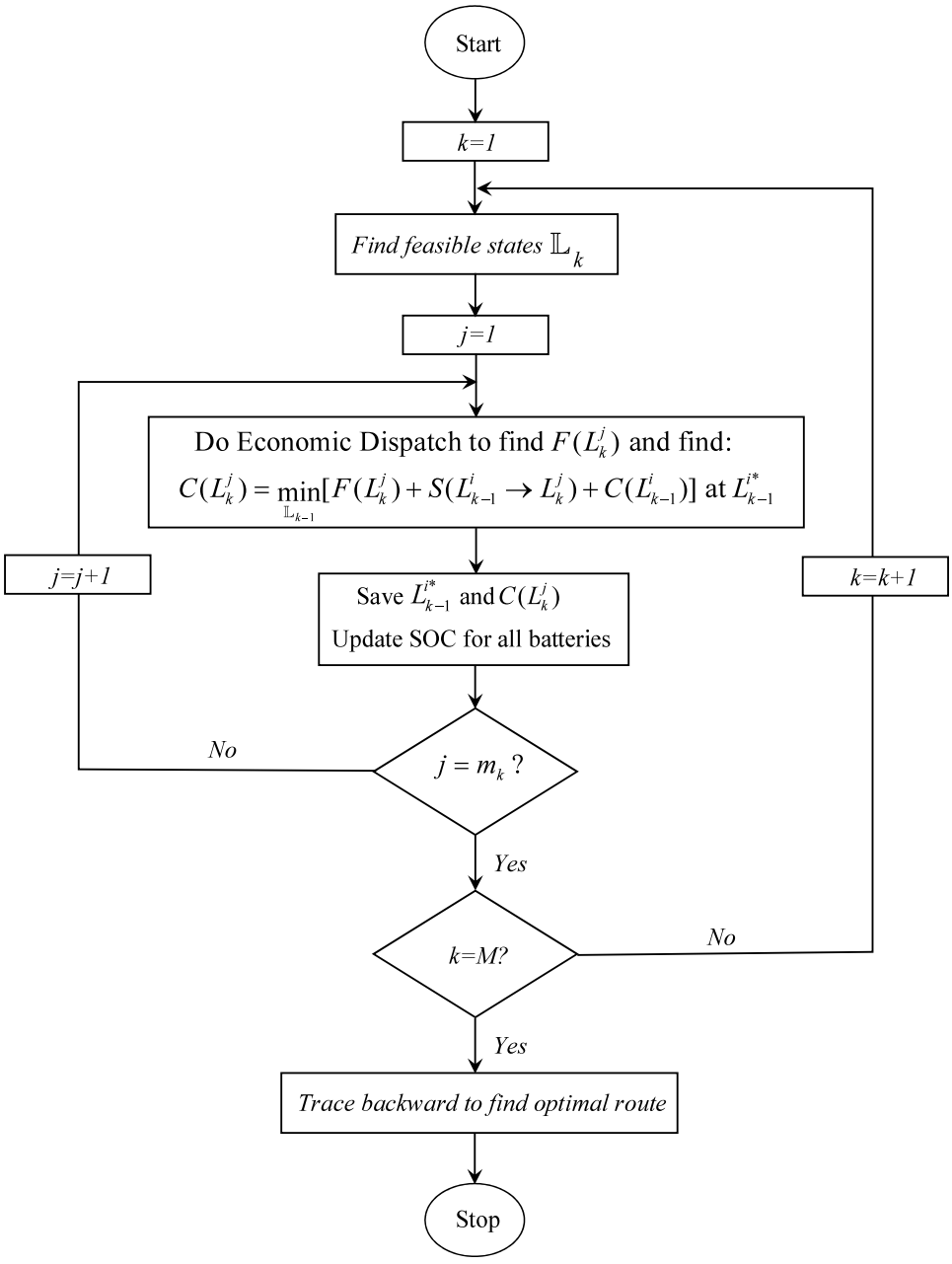

Fig. 2: Forward DP algorithm

IV. A CASE STUDY AND RESULTS

In this paper, a case study is developed to test the proposed approach. Fig. 3 shows a typical microgrid which connected to the low voltage side of a distribution transformer

to power the residential loads. The microgrid includes a $50kW$ diesel generator, $2 \times 20kW$ wind turbines, $50kW$ PV array, a $10kW/40kWh$ Vanadium Redox battery and an $12kW/30kWh$ AGM battery bank. The total load is $50kW$ at peak. The cost for AGM battery is estimated at $\$8000$. The replacement cost for the VRB is estimated at $\$20000$ (20% of the investment cost [27]).

The data of generator and batteries, extracted from manufacturers' data [28–30], and their initial states are given in Table.II and Table.III. Day-ahead forecast values of total load demands, PV and wind generations are given in Fig. 4 based on per-unit data from [31, 32]. The standard deviations for load, PV and wind power forecast errors are respectively 3.12%, 12.5% and 13.58% [33, 34]. α_k and β_k are chosen at 0.9 and 0.1 respectively.

TABLE II: Diesel generator data

a_{dg}	b_{dg}	c_{dg}	Start-up	c_{gen}
$3.10^{-4}\frac{gal/h}{kW^2}$	$0.052\frac{gal/h}{kW}$	$0.8gal/h$	$\$1$	$\$4/gal$
$T_{dg}^{up,min}$	$T_{dg}^{dw,min}$	P_{dg}^{min}	P_{dg}^{max}	Ini. state
$2hr$	$2hr$	$5kW$	$50kW$	$1hr$

TABLE III: Batteries data

	L_r	DOD_r	C_r	V_r
VRB	$10000cl$	50%	$40kWh$	$60V$
AGM	$1000cl$	50%	$30kWh$	$60V$
	SOC_{min}	SOC_{max}	Ini. SOC	kWh_f price
VRB	0.3	0.8	0.5	$0.1\$/kWh_f$
AGM	0.5	1	0.5	$0.59\$/kWh_f$

The standard deviations of the net load forecast error at each hour are calculated from (35) and given in Table.IV. The results for deterministic UC is shown in Fig. 5. By incorporating the operation cost functions of the batteries, ED tends to dispatch

TABLE IV: Net load forecast error standard deviation

$(k, \sigma_{net,k}(kW))$			
(1, 1.11)	(2, 1.06)	(3, 1.05)	(4, 1.04)
(5, 1.04)	(6, 0.64)	(7, 1.05)	(8, 0.81)
(9, 1.04)	(10, 2.54)	(11, 5.52)	(12, 6.27)
(13, 6.44)	(14, 5.50)	(15, 2.31)	(16, 1.36)
(17, 1.42)	(18, 1.6)	(19, 1.62)	(20, 1.80)
(21, 1.71)	(22, 1.42)	(23, 0.98)	(24, 0.67)

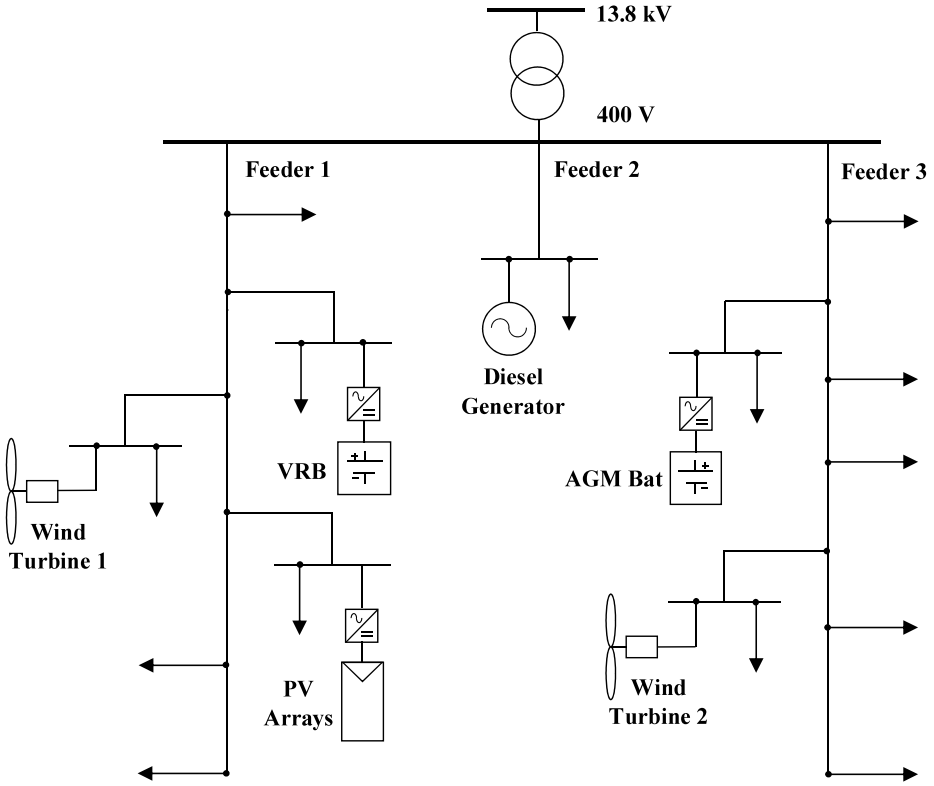

Fig. 3: A typical microgrid

power to the batteries which have with longer cycle life, lower replacement cost and higher efficiency. In this case, the VRB has lower kWh_f however the AGM battery has higher efficiency, therefore their dispatched powers, as shown in the results, are close.

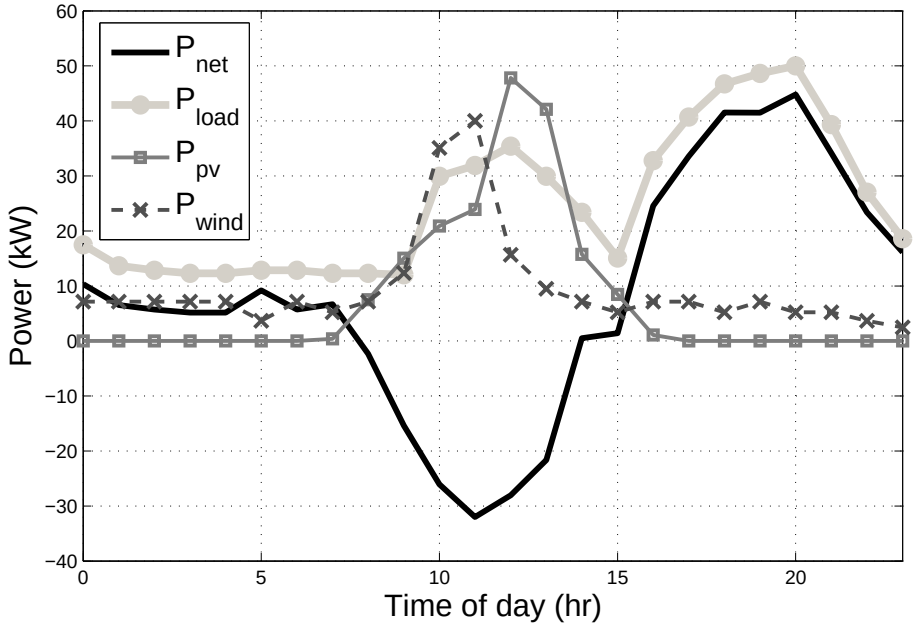

Fig. 4: Load and renewable power forecast

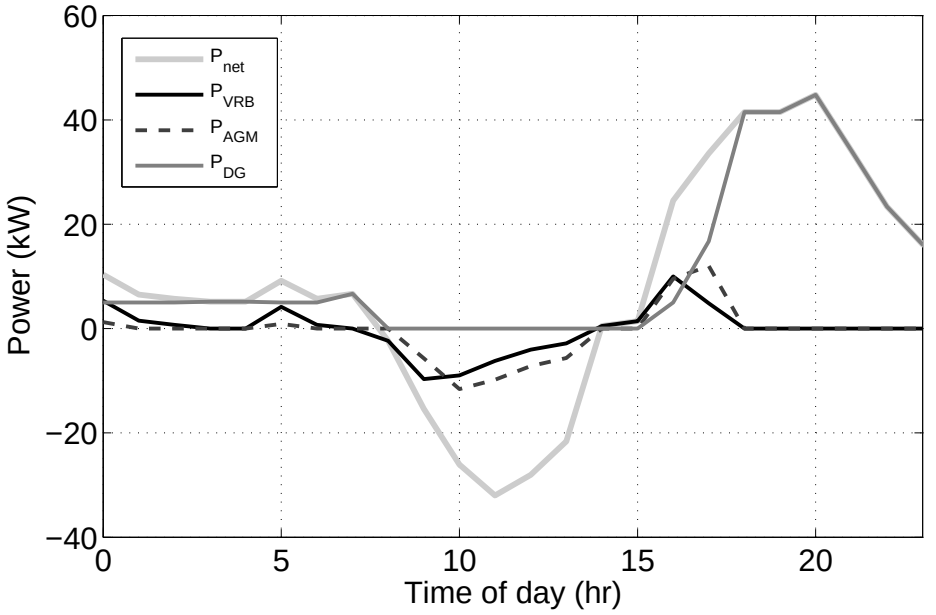

Fig. 5: Deterministic UC solution

Compared to the diesel generator, the batteries have lower operation cost due to lower fuel price and higher efficiency, however, the batteries are limited by their maximum DOD to have longer life cycle for AGM battery or to ensure that the VRB is working in linear region. For that reason, the batteries can only discharge for few hours at night, as seen in the results. The results for stochastic UC is shown in Fig. 6 in comparison with the deterministic case. Due to high α_k and low β_k as selected, the system dispatches more power to each unit. This is similar to assigning some amount of operating reserve to account for the uncertainties of load demands and renewable power forecast errors. The amount of reserve at each hour can be calculated via the enforcement of α_k and β_k. This is the advantage of the proposed stochastic approach over the conventional reserve requirement method which often assume the reserve requirement to be 30% of the forecast renewable generation[35].

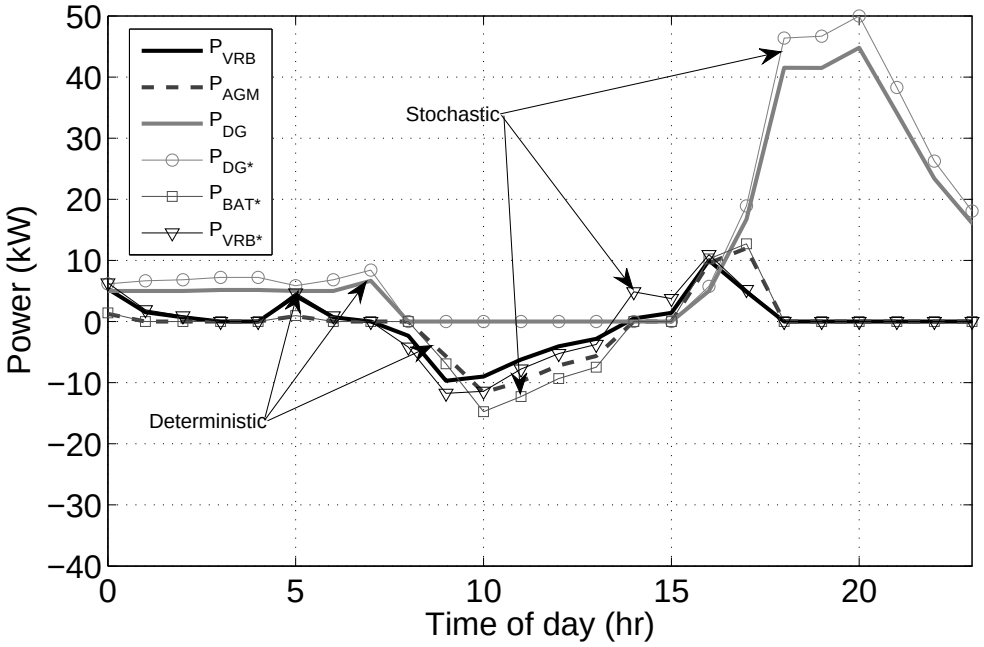

Fig. 6: Stochastic UC solution

V. CONCLUSIONS

In this paper, a novel battery operation cost model has been proposed. The model considers cycle life and charge/discharge efficiencies of the batteries. The model makes economic dispatch for multiple batteries possible in the microgrid system without introducing additional objective functions to maximize their efficiencies and their cycle lives. In addition, a probabilistic constrained approach has been proposed to consider the uncertainties in load and renewable power forecast errors. Stochastic dynamic programming is applied in this method to find the optimal day-ahead scheduling for a typical microgrid with a diesel generator, PV arrays, wind turbines, VRB and AGM batteries. Results show the proposed approach can maintain the system optimal operation with a high probability without investigating a vast number of scenarios. Future work in this area will include the consideration of electricity market price uncertainty into the stochastic UC and ED in which α_k and β_k need to be optimally selected to maximize the microgrid's profit.

References

[1] N. Hatziargyriou, Ed., *Microgrids: Architectures and Control*. Wiley, 2014.

[2] H. Liang and W. Zhuang, "Stochastic modeling and optimization in a microgrid: A survey," *Energies*, vol. 7, no. 4, pp. 2027–2050, 2014.

[3] B. F. W. Allen J. Wood, *Power Generation, Operation, and Control*. John Wiley & Sons INC., 1996, vol. 2nd.

[4] W. Su, J. Wang, and J. Roh, "Stochastic energy scheduling in microgrids with intermittent renewable energy resources," *Smart Grid, IEEE Transactions on*, vol. 5, no. 4, pp. 1876–1883, July 2014.

[5] X. Peng and P. Jirutitijaroen, "A probabilistic unit commitment problem with photovoltaic generation system," in *TENCON 2009 - 2009 IEEE Region 10 Conference*, Jan 2009, pp. 1–6.

[6] M. Lubin, C. G. Petra, M. Anitescu, and V. Zavala, "Scalable stochastic optimization of complex energy systems," in *High Performance Computing, Networking, Storage and Analysis (SC), 2011 International Conference for*. IEEE, 2011, pp. 1–10.

[7] G. Martinez, N. Gatsis, and G. B. Giannakis, "Stochastic programming for energy planning in microgrids with renewables," in *Computational Advances in Multi-Sensor Adaptive Processing (CAMSAP), 2013 IEEE 5th International Workshop on*. IEEE, 2013, pp. 472–475.

[8] S. Mohammadi, S. Soleymani, and B. Mozafari, "Scenario-based stochastic operation management of microgrid including wind, photovoltaic, micro-turbine, fuel cell and energy storage devices," *International Journal of Electrical Power & Energy Systems*, vol. 54, no. 0, pp. 525 – 535, 2014.

[9] T. Niknam, R. Azizipanah-Abarghooee, and M. R. Narimani, "An efficient scenario-based stochastic programming framework for multi-objective optimal micro-grid operation," *Applied Energy*, vol. 99, no. 0, pp. 455 – 470, 2012.

[10] M. Mazidi, A. Zakariazadeh, S. Jadid, and P. Siano, "Integrated scheduling of renewable generation and demand response programs in a microgrid," *Energy Conversion and Management*, vol. 86, no. 0, pp. 1118 – 1127, 2014.

[11] H. Bilil, G. Aniba, and M. Maaroufi, "Probabilistic economic emission dispatch optimization of multi-sources power system," *Energy Procedia*, vol. 50, no. 0, pp. 789 – 796, 2014.

[12] A. A. ElDesouky, "Security and stochastic economic dispatch of power system including wind and solar resources with environmental consideration," *International Journal of Renewable Energy Research-IJRER*, vol. 3, no. 4, 2013.

[13] Y. Tan, Y. Cao, C. Li, Y. Li, L. Yu, Z. Zhang, and S. Tang, "Microgrid stochastic economic load dispatch based on two-point estimate method and improved particle swarm optimization," *International Transactions on Electrical Energy Systems*, 2014.

[14] J. M. Lujano-Rojas, G. J. Osorio, and J. P. Catalao, "A probabilistic approach to

solve economic dispatch problem in systems with intermittent power sources," in *T&D Conference and Exposition, 2014 IEEE PES*, 2014, pp. 1–5.

[15] Y. Zhang, N. Gatsis, and G. B. Giannakis, "Risk-constrained energy management with multiple wind farms," in *Innovative Smart Grid Technologies (ISGT), 2013 IEEE PES*. IEEE, 2013, pp. 1–6.

[16] T. Nguyen and M. Crow, "Optimization in energy and power management for renewable-diesel microgrids using dynamic programming algorithm," in *Cyber Technology in Automation, Control, and Intelligent Systems (CYBER), 2012 IEEE International Conference on*, 2012, pp. 11–16.

[17] T. Nguyen, X. Qiu, J. Guggenberger II, M. Crow, and A. Elmore, "Performance characterization for photovoltaic-vanadium redox battery microgrid systems," *IEEE Transactions on Sustainable Energy*, vol. 5, no. 4, pp. 1379–1388, 2014.

[18] Rural fuel pricing in alaska. [Online]. Available: http://www.law.state.ak.us/pdf/civil/021810RuralFuelPricinginAlaska.pdf

[19] T. Markel, K. Smith, and A. Pesaran, "Improving petroleum displacement potential of phevs using enhanced charging scenarios," *EVS-24 NREL/CP-540-45730*, 2009.

[20] H. A. Kiehne, *Battery technology handbook*. CRC Press, 2003, vol. 60.

[21] O. Tremblay and L.-A. Dessaint, "Experimental validation of a battery dynamic model for ev applications," *World Electric Vehicle Journal*, vol. 3, no. 1, pp. 1–10, 2009.

[22] B. Hodge and M. Milligan, "Wind power forecasting error distributions over multiple timescales," in *Power and Energy Society General Meeting, 2011 IEEE*. IEEE, 2011, pp. 1–8.

[23] J. Wu, B. Zhang, H. Li, Z. Li, Y. Chen, and X. Miao, "Statistical distribution for wind power forecast error and its application to determine optimal size of energy storage system," *International Journal of Electrical Power & Energy Systems*, vol. 55, pp. 100–107, 2014.

[24] R. Doherty and M. O'Malley, "A new approach to quantify reserve demand in

systems with significant installed wind capacity," *IEEE Transactions on Power Systems*, vol. 20, no. 2, pp. 587–595, 2005.

[25] L. M. Costa and G. Kariniotakis, "A stochastic dynamic programming model for optimal use of local energy resources in a market environment," in *Power Tech, 2007 IEEE Lausanne*. IEEE, 2007, pp. 449–454.

[26] D. P. Bertsekas, *Dynamic programming: deterministic and stochastic models*, D. P. Bertsekas, Ed. Prince-Hall, 1987.

[27] G. Kear, A. A. Shah, and F. C. Walsh, "Development of the all-vanadium redox flow battery for energy storage: a review of technological, financial and policy aspects," *International Journal of Energy Research*, vol. 36, no. 11, pp. 1105–1120, 2012.

[28] MQ Power. [Online]. Available: http://www.powertechengines.com/MQP-DataSheets/MQP050IZ_Rev_0.pdf

[29] Prudent Energy. [Online]. Available: http://www.pdenergy.com/pdfs/Prudent_Energy_Product_Brochure_2011.pdf

[30] Sunxtender. [Online]. Available: http://www.sunxtender.com/solarbattery.php?id=11

[31] D. Hung, N. Mithulananthan, and K. Lee, "Determining PV penetration for distribution systems with time-varying load models," *IEEE Transactions on Power Systems*, to be published, early Access.

[32] A. A. Moghaddam, A. Seifi, and T. Niknam, "Multi-operation management of a typical micro-grids using particle swarm optimization: A comparative study," *Renewable and Sustainable Energy Reviews*, vol. 16, no. 2, pp. 1268–1281, 2012.

[33] N. Lu, R. Diao, R. Hafen, N. Samaan, and Y. Makarov, "A comparison of forecast error generators for modeling wind and load uncertainty," in *Power and Energy Society General Meeting (PES), 2013 IEEE*, 2013, pp. 1–5.

[34] F. Kreikebaum, R. Moghe, A. Prasai, and D. Divan, "Evaluating the application of energy storage and day-ahead solar forecasting to firm the output of a photovoltaic plant," in *Energy Conversion Congress and Exposition (ECCE), 2011 IEEE*, 2011, pp. 3556–3561.

[35] A. Zakariazadeh and S. Jadid, “Energy and reserve scheduling of microgrid using multi-objective optimization,” in *Electricity Distribution (CIRED 2013), 22nd International Conference and Exhibition on*, 2013, pp. 1–4.

2. CONCLUSIONS

In this dissertation, three papers have been proposed solve three problems including: microgrid systems performance characterization, optimal sizing for energy storage system and stochastic optimization of microgrid operation. In the first paper, a PV-VRB microgrid system performance has been characterized. The system operating characteristics, losses, and efficiencies are quantified and formulated based on measured data. The VRB discharge and charge efficiencies are found to be nonlinear with the load/charge power. Based on the system characterization, a scalable model has been built to accurately predict the system behavior and performance. A case study has been performed for May 2013. In second paper, an analytical approach has been developed for optimal sizing of VRB storage system for isolated microgrids. Non-linear charge/discharge efficiencies and operating characteristics of VRB system are considered in the system's constraints. The feasibility of the solution is ensured based on per-day cost model. The method can also be valid for optimal sizing different types of ESSs if the cost and efficiency model are known. Case studies have been performed to find optimal VRB power and energy ratings for both isolated and grid-connected microgrids considering different scenarios of load and insolation. The results show the optimal solution occurs when the operating cost benefit by increasing VRB capacity can justify the increment in investment capital. In the third paper, a novel battery operation cost model has been proposed. The model considers cycle life and charge/discharge efficiencies of the batteries. The model makes economic dispatch for multiple batteries possible in the microgrid system without introducing additional objective functions to maximize their efficiencies and their cycle lives. In addition, a probabilistic constrained approach has been proposed to consider the uncertainties in load and renewable power forecast errors. Stochastic dynamic programming is applied in this method to find the optimal day-ahead scheduling for a typical microgrid with a diesel generator, PV arrays, wind turbines, VRB and AGM batteries. Results show the proposed approach can

maintain the system optimal operation with a high probability without investigating a vast number of scenarios. Future work in this area will include the consideration of electricity market price uncertainty into the stochastic UC and ED in which α_k and β_k need to be optimally selected to maximize the microgrid's profit.

VITA

Tu Anh Nguyen obtained his B.S. in Electrical Engineering from Hanoi University of Technology (currently Hanoi University of Science and Technology) in July 2007. He received his Ph.D. in Electrical Engineering from Missouri University of Science and Technology in December 2014.

Tu Nguyen was employed as a graduate research assistant at the Missouri University of Science and Technology under Dr. Mariesa L. Crow from 2009 to 2014. During this time, he was part of a team that designed and built three working renewable-energy microgrids, as well as completed research which led to this dissertation. From 2008 to 2009, Tu Nguyen worked as an Power Transformer Test Engineer at ABB Ltd. Vietnam.

Tu Nguyen is a member of The Institute of Electrical and Electronics Engineers (IEEE) and IEEE Power and Energy Society (PES).